THE ASTROPHYSICAL JOURNAL, 424:772–792, 1994 April 1

CHEMICAL TRANSITIONS FOR INTERSTELLAR C_2 AND CN IN CLOUD ENVELOPES

S. R. FEDERMAN,[1,2,3] C. J. STROM,[1] D. L. LAMBERT,[4] JASON A. CARDELLI,[5,6]
V. V. SMITH,[4,6] AND C. L. JOSEPH[7]

Received 1993 January 19; accepted 1993 October 6

ABSTRACT

Observations were made of absorption from CH, C_2, and CN toward moderately reddened stars in Sco OB2, Cep OB3, and Taurus/Auriga. For these directions, most of the reddening is associated with a single cloud complex, for example, the ρ Ophiuchus molecular cloud, and as a result, the observations probe moderately dense material. When combined with available data for nearby directions, the survey provides the basis for a comprehensive analysis of the chemistry for these species.

The chemical transitions affecting C_2 and CN in cloud envelopes were analyzed. The depth into a cloud at which a transition takes place was characterized by τ_{uv}, the grain optical depth at 1000 Å. One transition at $\tau_{uv} \sim 2$, which arises from the conversion of C^+ into CO, affects the chemistries for both molecules because of the key role this ion plays. A second one involving production terms in the CN chemistry occurs at τ_{uv} of ~ 3; production via ion-molecule reactions with NH dominates at lower optical depths, while that via neutral-neutral reactions which C_2 and CH is more important at larger values for τ_{uv}. The transition from photodissociation to chemical destruction takes place at $\tau_{uv} \sim 4.5$ for C_2 and CN.

The observational data for stars in Sco OB2, Cep OB3, and Taurus/Auriga were studied with chemical rate equations containing the most important production and destruction mechanisms. Because the sample of stars in Sco OB2 includes sight lines with A_v ranging from 1–4 mag, sight lines dominated by photochemistry could be analyzed separately from those controlled by gas-phase destruction. The analysis yielded values for two poorly known rate constants for reactions involved in the production of CN; the reactions are $C_2 + N \rightarrow CN + C$ and $C^+ + NH \rightarrow$ all products. The other directions were analyzed with the inferred values. The predicted column densities for C_2 and CN agree with the observed values to better than 50%, and in most instances 20%. When combining the estimates for density and temperature derived from chemical modeling and molecular excitation for a specific cloud, such as the ρ Ophiuchus molecular cloud, the portion of the cloud envelope probed by C_2 and CN absorption was found to be in pressure equilibrium.

Subject headings: ISM: clouds — ISM: molecules — molecular processes

1. INTRODUCTION

Several types of chemical transitions take place in cloud envelopes. The most basic of these are transitions from atomic to molecular gas. Two particular examples are the H I to H_2 transition and the C^+ to CO transition. Both of these arise when the principal destruction route for the molecule, photodissociation, is suppressed by self-shielding as the molecular lines involved in photodissociation become optically thick. These transitions were studied in detail theoretically by Federman, Glassgold, & Kwan (1979) for hydrogen and by Bally & Langer (1982), Glassgold, Huggins, & Langer (1985), van Dishoeck and Black (1988), and Viala et al. (1988a) for CO. Glassgold & Langer (1975) analyzed the gas-phase chemistry involved in the C^+ to CO transition. The emphasis in the present paper is placed on somewhat different types of chemical transitions, those occurring among production and destruction terms for the chemistries of C_2 and CN in the diffuse envelopes of interstellar clouds.

Our analysis is based on newly acquired data and information available in the literature on absorption from CH, C_2, and CN along many lines of sight, including some with A_v, total visual extinction, approaching 4 mag. Our focus is on several directions within specific star-forming complexes; the regions included in this study are the Scorpius OB2 association and the ρ Ophiuchus molecular cloud, the Cepheus OB3 association and its parent cloud, Cepheus A, and the stars behind dark clouds in Taurus and Auriga. This study, which is a synthesis of several methods used in the past for analyses of gas toward lines of sight with $A_v < 1$ mag, enables us to obtain a more global picture for a given interstellar cloud based solely on optical data. It should be noted that although there is up to 4 mag of visual extinction to stars in our survey, the sight lines usually sample a single cloud or complex.

Most previous studies on the chemistry occuring in the diffuse envelopes of clouds involved one of two complementary approaches. One approach relies on a comprehensive analysis of the atomic and molecular material observed along a specific line of sight toward a background star. An objective in such analyses is the determination of density and temperature for the gas and of the flux of ultraviolet radiation permeating the cloud. Theoretical efforts in this vein include the work on the diffuse clouds toward ζ Ophiuchi by Black & Dalgarno (1977), van Dishoeck & Black (1986), and Viala, Roueff, & Abgrall (1988b) and the work on material toward γ Ara by Federman

[1] Department of Physics and Astronomy, University of Toledo, Toledo, OH 43606.
[2] Jet Propulsion Laboratory, California Institute of Technology, 4800 Oak Grove Drive, Pasadena, CA 91109.
[3] Guest Observer, McDonald Observatory, University of Texas at Austin.
[4] Department of Astronomy, University of Texas, Austin, TX 78712.
[5] Department of Astronomy, University of Wisconsin, Madison, WI 53706.
[6] Visiting Astronomer, Kitt Peak National Observatory, National Optical Astronomy Observatories (NOAO). NOAO are operated by the Association of Universities for Research in Astronomy, Inc., under cooperative agreement with the National Science Foundation.
[7] Department of Astrophysical Sciences, Princeton University, Princeton, NJ 08544.

& Glassgold (1980). Van Dishoeck & Black (1986) also modeled the gas toward o Per, ζ Per, and χ Oph. A common thread among these investigations is that each of the lines of sight has at most $E(B-V) \sim 0.33$ mag of reddening, or $A_v \sim 1$ mag, and thus the clouds are permeated by ultraviolet radiation. More reddened directions have been studied recently by Nercessian, Benayoun, & Viala (1988a), who modeled the gas toward HD 29647, Januzzi et al. (1988), who studied the gas toward HD 169454, and van Dishoeck & Black (1989), who presented models for the gas toward HD 29647 and HD 147889. In these directions, the chemistry resembles that in the cores of dense clouds where gas-phase processes (e.g., ion-molecule reactions) rather than photoprocesses control the chemistry.

The second approach focuses on the chemistry of a single molecule through observations of many lines of sight. Previous studies of this kind examined the chemistry of CO (Federman et al. 1980), of CH (Federman 1982; Danks, Federman, & Lambert 1984; Crawford 1989), and of CN (Federman, Danks, & Lambert 1984). Danks & Lambert (1983), van Dishoeck & de Zeeuw (1984), van Dishoeck & Black (1989), and Gredel, van Dishoeck, & Black (1993) investigated the rotational excitation and the chemistry of C_2 through this approach. As with most of the previous modeling efforts, many of these observationally based studies examined specific clouds with A_v less than 1 mag.

In this paper, the analysis is a synthesis of the two approaches. The available chemical models are refined through a study of the CN radical, and to some extent the C_2 molecule, for sight lines sampling A_v of 1–4 mag and associated with a single cloud. The cloud along each line of sight is modeled so that the most consistent chemical picture emerges. This picture results in refined values for density, temperature, and flux of radiation, and the physical conditions are described in a global context for each cloud complex. By combining the analyses for several cloud complexes, we are able to examine the chemical transitions involving production and destruction terms for C_2 and CN.

The remainder of the paper has the following outline. The next section describes our data and § 3 presents the observational results. The chemical model, the examination of chemical transitions, and analysis of the observational work are described in § 4; this is followed by a general discussion. The final section presents a summary of our conclusions and directions for future work.

2. DATA

Moderate-resolution spectroscopic observations were acquired from McDonald Observatory, Kitt Peak National Observatory, and the Canadian-French-Hawaiian Telescope. Most of the data for CH, C_2, and CN were obtained at McDonald. The next sections describe the details of the measurements for each facility. Table 1 provides information about each of our program stars.

2.1. *McDonald Observatory*

These observations were made with the coudé spectrometer on the 2.1 m telescope over the period from 1987 July to 1990 January. There were three basic setups: one for CH at 4300 Å, one for C_2 at 8760 Å, and one for CN and CH at 3880 Å. In each case, a grating was used to disperse the light; a $CuSO_4$ filter and an RG 715 filter were used in the blue and the red,

TABLE 1

PROGRAM STARS

HD/BD	Name	Spectral Type	V	$E(B-V)$	Comments
21291	...	B9 Ia	4.21	0.42	
21483	...	B3 III	7.06	0.56	Near NGC 1333
23512	...	A0 V	8.11	0.36	Behind Pleiades cloud
26571	...	B8 III	6.10	0.29	
27405	...	B5 V	7.79	0.34	Near L1506
27778	62 Tau	B3 V	6.17	0.40	Near L1506
28975	...	A5 III	8.75	0.73	Behind TMC-2
29309	...	B2 V	7.08	0.5:	
29334	...	A2 IV	8.96	0.60	Near HCL-2
31293	AB Aur	2B9 IV	7.10	0.18	In L1517, outflow source
34078	AE Aur	O9.5 V	5.30	0.52	
37903	...	B1.5 V	7.82	0.35	Illuminates NGC 2023
53367	...	B0 IVe	6.97	0.74	
73882	...	O8.5 V	7.19	0.72	
147009	...	B9.5 V	8.08	0.33	Illuminates vdB102
147701	...	B5 V	8.35	0.72	Behind ρ Oph Cloud
147888	ρ Oph D	B5 V	6.74	0.47	Behind ρ Oph Cloud
147932	ρ Oph C	B5 V	7.27	0.48	Behind ρ Oph Cloud
−14°5037	...	B1.5 Ia	8.24	1.59	Distant supergiant
169454	...	B1 Ia$^+$	6.60	1.16	Distant supergiant
179406	20 Aql	B3 V	5.37	0.33	
184915	κ Aql	B0.5 III	4.96	0.26	
200775	...	Be Vp	7.20	0.44	Iluminates NGC 7023
206165	9 Cep	B2 Ib	5.04	0.47	
210072	...	B 8	7.8	0.46	
216532	...	O8 V	8.03	0.86	Behind Cep A Cloud
216658	...	B0.5 V	8.91	0.98	Behind Cep A Cloud
216898	...	O8.5 V	8.04	0.85	Behind Cep A Cloud
217061	...	B1 V	8.79	0.96	Behind Cep A Cloud
217086	...	O7 V	7.66	0.96	Behind Cep A Cloud
217312	...	B0.5 V	7.42	0.66	Behind Cep A Cloud

respectively, to block light from unwanted spectral orders. The detector was either an RCA CCD with 30 μm pixels or a Tektronics CCD with 27 μm pixels. The resolving power ($\lambda/\delta\lambda$), which is determined by the grating/detector combination, was typically 25,000 to 30,000, except for the observations at 4300 Å, where the value was $\sim$15,000. These resolving powers were derived from spectral calibration sources, which had typical line widths of 2.5 pixels. The calibration sources used in the measurements were either an iron arc or hollow cathode lamps containing mixtures of Fe/Ne, Fe/Ar, and Th/Ar. It should be noted that the aim of the survey was not to obtain accurate wavelengths (or velocities) for the interstellar absorption, but instead to seek absorption from individual clouds with more reddening than were typically studied by us previously.

The data were reduced with the aid of two packages. For the earliest data (1987 July and 1988 January), the data were processed with software from the WFPC-2 team at the Jet Propulsion Laboratory; the remaining data were processed with NOAO's IRAF package. Although different packages were used, the data were reduced in a similar fashion. The bias level was subtracted from the spectral images, and the stellar spectra were divided by a flat field to remove pixel-to-pixel variations in sensitivity. Then rows perpendicular to the dispersion were summed, and the wavelength scale was determined by the calibration arcs and hollow cathode lamps. The equivalent widths were measured with a planimeter for the earliest data and with the Gaussian-fitting routine within IRAS. Approximate wavelengths at line center (with typical errors in velocity of $\sim$2–3 km s^{-1}) were obtained in all instances by Gaussian fits. The main purpose for this latter step was to check the identity of a line with other available data on interstellar velocities along the line of sight. We found that at our moderate resolution, we had to limit our observations to spectral types earlier than about B8 in order to avoid confusion with stellar metal lines. Two sample spectra are shown in Figure 1.

Additional observations of HD 28975 in the vicinity of the CN lines were made with the coudé spectrograph on the 2.7 m telescope. In this case, a TI CCD with 15 μm pixels was used to obtain spectra for CN at 3880 Å; the resolving power with the TI CCD was set to 26,000.

2.2. *Kitt Peak National Observatory*

Spectra toward the Cep OB3 association were obtained at Kitt Peak National Observatory with the 4 m telescope plus Cassegrain echelle spectrometer and the blue long-camera. Grating 31-63 was used along with cross disperser 226-2 and the RCA2 CCD detector with 512 × 320 30 μm square pixels. A two pixel slit-width (at the CCD) set the resolving power of the spectrometer to 35,000 and the wavelength coverage was incomplete over the interval 3800–4400 Å. The data were reduced to one-dimensional spectra using IRAF. Bias subtraction was done using separate sets of bias frames taken at the beginning and end of each night and pixel-to-pixel sensitivity variations were removed by dividing each frame by a quartz flat-field lamp. Individual orders were traced and summed to yield separate one-dimensional spectra with wavelength scales set using a Th/Ar hollow cathode lamp; the wavelength scale is accurate to about 0.01 Å.

For some of the Cep OB3 stars, we have additional McDonald spectra at resolving powers of 80,000 for lines of CH, CH$^+$, and Ca I, and a comparison between the Kitt Peak and McDonald spectra (smoothed to the lower Kitt Peak resolution) reveals excellent agreement in the line profiles and integrated equivalent widths.

2.3. *Canadian-France-Hawaiian Telescope*

Additional data on interstellar CN and CH for stars previously observed by Joseph, Snow, and Seab (1989) were incorporated into this survey. Besides the $R(0)$ line of CN,

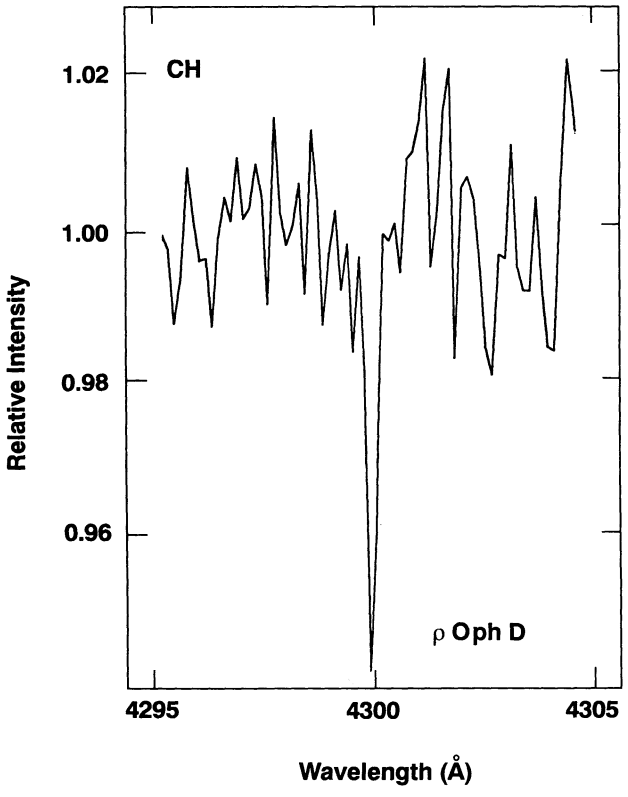

FIG. 1a

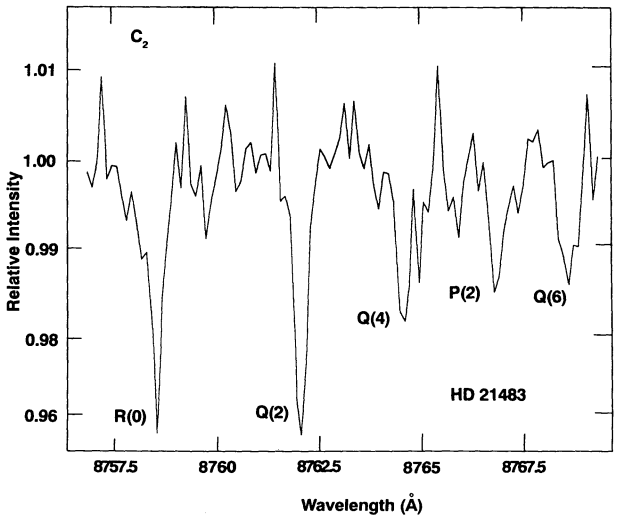

FIG. 1b

FIG. 1.—Representative spectra: (*a*) CH λ4300 toward ρ Oph D and (*b*) C_2 toward HD 21483 with individual rotational levels indicated

which was analyzed previously, the $R(1)$ and $P(1)$ lines of CN and the $R_2(1)$ line of CH were examined by us. All the data were reduced with a third-generation software package called MSLAP recently developed by C. Joseph and E. Jenkins. Details of the observations can be found in Joseph et al.; here we note the salient points. The detector was a 1872-element Reticon array with 27 μm pixels, and the resolution was found to be 0.074 Å over 2 pixels, corresponding to a resolving power of $\sim$50,000.

3. OBSERVATIONAL RESULTS

Tables 2 and 3 present the measured equivalent widths (W_λ) and the derived column densities for the transitions of CN and CH and of C_2, respectively. The quoted uncertainty in W_λ represents 1 σ errors, which were calculated with the expression in Jenkins et al. (1973). The signal-to-noise ratio was obtained from the fluctuations in the stellar continuum in the vicinity of the interstellar line and was found to have a typical

TABLE 2

RESULTS FOR CN AND CH

		HD 21291		HD 21483		HD 23512		HD 26571	
λ (Å)	f-VALUE	W_λ (mÅ)	N (cm^{-2})	W_λ (mÅ)	N (cm^{-2})	W_λ (mÅ)	N (cm^{-2})	W_λ (mÅ)	N (cm^{-2})
					CN				
3874.61	0.0342	7.7 ± 0.2	1.9(12)[a]	39.2 ± 3.3	3.3(13)	≤10.	≤2.6(12)	...	...
3874.00	0.0228	2.0 ± 0.2	6.8(11)	17.0 ± 2.5	7.8(12)	...	...	...	...
3875.76	0.0114	1.2 ± 0.2	8.1(11)	12.6 ± 2.8	1.0(13)	...	...	...	...
N(CN)			2.6(12)		4.2(13)		≤3.9(12)[b]		...
					CH				
4300.31	0.0051	...	...	25.7 ± 1.3	5.1(13)	5.3 ± 0.8	6.9(12)	10.3 ± 1.2	1.4(13)
3886.41	0.0033	...	...	9.1 ± 1.4	2.4(13)	≤8.0	≤2.1(13)	...	...
3890.21	0.0022	...	...	≤7.2	≤2.8(13)	...	...	...	...
3878.77	0.0011	1.0 ± 0.2	6.9(12)	≤2.5	≤1.8(13)	...	...	...	...
N(CH)			2.1(13)[c]		4.2(13)		6.9(12)		1.4(13)

		HD 27405		HD 27778		HD 28975		HD 29309	
λ (Å)	f-VALUE	W_λ (mÅ)	N (cm^{-2})	W_λ (mÅ)	N (cm^{-2})	W_λ (mÅ)	N (cm^{-2})	W_λ (mÅ)	N (cm^{-2})
					CN				
3874.61	0.0342	13.0 ± 3.2	3.6(12)	27.3 ± 0.5	1.2(13)	30.0 ± 6.0	1.4(13)	13.6 ± 0.9	3.8(12)
3874.00	0.0228	...	...	10.5 ± 0.5	4.2(12)	11.0 ± 3.0	4.4(12)	5.0 ± 0.8	1.8(12)
3875.76	0.0114	...	...	4.9 ± 0.4	3.5(12)	≤12.	≤9.8(12)	≤3.0	≤2.1(12)
N(CN)			5.4(12)[b]		1.6(13)		1.8(13)		5.6(12)
					CH				
4300.31	0.0051	17.9 ± 1.8	2.9(13)	21.7 ± 0.6	3.9(13)	50.0 ± 4.0	4.0(14)	...	...
3886.41	0.0033	≤7.8	≤2.0(13)	6.7 ± 0.8	1.7(13)	31.0 ± 6.0	1.7(14)	...	...
3890.21	0.0022	...	...	≤2.8	≤9.9(12)	≤12.	≤5.1(13)	...	...
3878.77	0.0011	...	...	≤3.5	≤2.5(13)	≤12.	≤1.0(14)	≤2.6	≤1.9(13)
N(CH)			2.9(13)		2.7(13)		2.2(14)		≤5.7(13)[c]

		HD 29334		AB Aur		AE Aur		HD 37903	
λ (Å)	f-VALUE	W_λ (mÅ)	N (cm^{-2})	W_λ (mÅ)	N (cm^{-2})	W_λ (mÅ)	N (cm^{-2})	W_λ (mÅ)	N (cm^{-2})
					CN				
3874.61	0.0342	...	...	≤4.1	≤9.7(11)	8.7 ± 1.7	2.2(12)	≤12.	≤3.3(12)
3874.00	0.0228	...	...	...	...	...	...	...	...
3875.76	0.0114	...	...	...	...	...	...	...	...
N(CN)			...		≤1.5(12)[b]		3.3(12)[b]		≤5.0(12)[b]
					CH				
4300.31	0.0051	25.9 ± 2.9	5.2(13)	≤3.0[e]	≤3.8(12)	...	...	≤7.8[e]	≤1.1(13)
3886.41	0.0033	...	...	≤1.0[e]	≤2.3(12)	17.0 ± 1.5	5.4(13)	≤14.	≤4.1(13)
3890.21	0.0022	...	...	...	...	14.9 ± 2.2	6.7(13)	...	...
3878.77	0.0011	...	...	...	...	...	...	...	...
N(CH)			5.2(13)		≤2.3(12)		1.2(14)		≤1.1(13)

TABLE 2—*Continued*

λ (Å)	*f*-VALUE	HD 53367 W_λ (mÅ)	HD 53367 N (cm^{-2})	HD 73882 W_λ (mÅ)	HD 73882 N (cm^{-2})	HD 147009 W_λ (mÅ)	HD 147009 N (cm^{-2})	ρ Oph D W_λ (mÅ)	ρ Oph D N (cm^{-2})
				CN					
3874.61	0.0342	14.1 ± 2.0	4.0(12)	18.0 ± 2.0[d]	5.7(12)	...	...	...	...
3874.00	0.0228	≤6.0	≤2.2(12)	25.0 ± 3.0	1.5(13)	...	...	...	...
3875.76	0.0114	≤4.1	≤2.9(12)	13.0 ± 3.0	1.1(13)	...	...	...	...
N(CN)			6.2(12)		>1.9(13)		...		...
				CH					
4300.31	0.0051	...	...	...	...	8.8 ± 2.8	1.2(13)	17.6 ± 3.1	2.9(13)
3886.41	0.0033	...	...	...	...	...	...	...	...
3890.21	0.0022	...	...	...	...	...	...	...	...
3878.77	0.0011	≤7.6	≤5.9(13)	5.6 ± 2.8	4.2(13)	...	...	...	...
N(CH)			≤1.8(14)[e]		1.3(14)[e]		1.2(13)		2.9(13)

λ (Å)	*f*-VALUE	ρ OPH C W_λ (mÅ)	ρ OPH C N (cm^{-2})	BD −14°5037 W_λ (mÅ)	BD −14°5037 N (cm^{-2})	HD 169454 W_λ (mÅ)	HD 169454 N (cm^{-2})	HD 200775 W_λ (mÅ)	HD 200775 N (cm^{-2})	HD 210072 W_λ (mÅ)	HD 210072 N (cm^{-2})
					CN						
3874.61	0.0342	7.4 ± 2.1	1.8(12)	...	...	22.4 ± 3.1	8.0(12)	...	...	18.6 ± 3.6	6.0(12)
3874.00	0.0228	≤4.8	≤1.7(12)	...	...	11.2 ± 3.3	4.5(12)	...	...	8.9 ± 4.0	3.4(12)
3875.76	0.0114	6.3 ± 2.3	4.6(12)	...	...	5.9 ± 3.9	4.3(12)	...	...	≤11.7	≤9.5(12)
N(CN)			2.7(12)[b]		...		1.2(13)		...		9.4(12)
					CH						
4300.31	0.0051	14.1 ± 2.8	2.1(13)	47.3 ± 6.9	3.0(14)	34.7 ± 3.0	9.5(13)	23.4 ± 2.7	4.4(13)	...	...
3886.41	0.0033	≤5.7	≤1.4(13)	...	...	14.9 ± 3.5	4.5(13)	...	...	...	...
3890.21	0.0022	≤9.7	≤3.9(13)	...	...	≤6.4	≤2.4(13)	...	...	...	...
3878.77	0.0011	≤4.5	≤3.3(13)	...	...	≤7.7	≤6.0(13)	...	...	...	...
N(CH)			2.1(13)		3.0(14)		6.9(13)		4.4(13)		...

[a] 1.9 (12) = 1.9×10^{12}.
[b] When CN data were lacking, *N*(CN) was set equal to 1.5 times the value from λ3874.6, a typical value for positive detections.
[c] When CH data were lacking, *N*(CH) was set equal to 3 times the value for λ3878.8, a typical value for positive detections.
[d] Data were affected by cosmic-ray hit.
[e] Possible stellar contamination.

value of 100–200. For the stars in common with other studies, such as Gredel, van Dishoeck, & Black (1991), our W_λ's are for the most part consistent with earlier measures. For HD 23512, we believe that the difference between our result for CH λ4300 and that of White (1984) arises because he did not consider the presence of stellar contamination. The column densities were usually determined from curves of growth (Strömgren 1948; Münch 1968) with a Gaussian shape for the line profile and a *b*-value of 1 km s^{-1}. Neither Λ-doubling in CH nor hyperfine splitting in CN were explicitly considered because the effects were small for our sample. The oscillator strengths are the same as those used by us previously (CH, Danks et al. 1984; CN, Federman et al. 1984; C_2, Danks & Lambert 1983). The adopted *b*-value is consistent with the value derived in other studies of molecular absorption (e.g., Gredel, van Dishoeck, & Black 1991).

The determination of column densities for CH and C_2 was aided by the presence of several lines. For CH, when the *A*–*X* and *B*–*X* transitions were both observed, the column density was taken to be the average of the two results. The result for the *A*–*X* transition was used when only an upper limit to λ3886, the strongest line in the *B*–*X* transition, was obtained. Furthermore, when only CH λ3878 was available, as was the case for the CFHT observations, the column density was estimated by multiplying the result for the line by 3, instead of the expected factor of 2, because for many sight lines, column densities from each $T_{2e}(\frac{1}{2})$ state were found to be about one-half the column densities of the $T_{2f}(\frac{1}{2})$ states measured by λ3886—for example, see Table 2. The small sample for which this correction applies does not affect any of our conclusions. For C_2, the presence of two or three lines from a given rotational level in the ground electronic state provided a check on the results for that level, and the presence of transitions from levels $J = 0$ to $J = 8$ provided a means of estimating the excitation temperature (T_{ex}) for the molecule. We estimated T_{ex} from a least-squares fit to the data; the value for T_{ex} is given in Table 3. The excitation temperature was then used to determine the amount of C_2 in higher rotational levels than those studied and these amounts are indicated in the table as italics. The total column density given in the table includes the contribution from these levels. An example of the analysis for the gas toward 20 Aql is shown in Figure 2, where the excitation temperature is obtained from the dashed line. The solid lines are theoretical results from van Dishoeck & Black (1982), which provide an estimate of density, $n_c = n(H) + n(H_2)$, from the ratio $n_c\ \sigma/I_{ir}$. Here, σ is the collisional de-excitation cross section and I_{ir} is

TABLE 3

RESULTS FOR C_2

LINE	λ (Å)	f-VALUE	HD 21483 W_λ (mÅ)	HD 21483 N (cm^{-2})	HD 26571 W_λ (mÅ)	HD 26571 N (cm^{-2})	HD 27778 W_λ (mÅ)	HD 27778 N (cm^{-2})	AE Aur W_λ (mÅ)	AE Aur N (cm^{-2})
$R(0)$	8757.686	1.0(−3)[a]	9.3 ± 1.2	1.4(13)	4.2 ± 1.0	6.2(12)	2.6 ± 0.7	3.8(12)	≤2.0	≤2.9(12)
$N(0)$			1.4(13)		6.2(12)		3.8(12)		≤2.9(12)	
$R(2)$	8753.949	4.0(−4)	5.1 ± 1.6	1.9(13)	7.3 ± 1.1	2.7(13)	≤2.0	≤2.4(12)	4.2 ± 1.0	1.6(13)
$Q(2)$	8761.194	5.0(−4)	11.5 ± 1.3	3.5(13)	8.2 ± 1.1	2.4(13)	≤1.8	≤5.3(12)	3.2 ± 0.7	9.4(12)
$P(2)$	8766.031	1.0(−4)	5.6 ± 1.2	8.2(13)	...	...	...	...	...	...
$N(2)$			2.7(13)		2.6(13)		≤5.3(12)		1.3(13)	
$R(4)$	8751.685	3.33(−4)	...	...	7.3 ± 1.2	3.3(13)	...	...	3.4 ± 0.9	1.5(13)
$Q(4)$	8763.751	5.0(−4)	7.0 ± 1.3	2.1(13)	~10[d]	3.0(13)	3.7 ± 0.9	1.1(13)	5.3 ± 0.6	1.6(13)
$P(4)$[e]	8773.430	1.67(−4)	...	...	...	...	...	...	...	...
$N(4)$			2.1(13)		3.2(13)		1.1(13)		1.6(13)	
$R(6)$	8750.848	3.08(−4)	...	...	...	...	...	...	...	...
$Q(6)$	8767.759	5.0(−4)	8.1 ± 1.6[f]	2.4(13)	...	...	2.9 ± 0.9	8.5(12)	4.6 ± 0.7	1.4(13)
$P(6)$	8782.308	1.92(−4)	...	...	...	...	...	...	...	...
$N(6)$			2.4(13)		*2.5(13)*[g]		8.5(12)		1.4(13)	
$Q(8)$[e]	8773.221	5.0(−4)	≤2.4	≤7.1(12)	...	...	≤2.4	≤7.1(12)	...	...
$N(8)$			≤7.1(12)		*1.4(13)*		≤7.1(12)		*8.8(12)*	
$N(10)$			*1.0(12)*		*4.4(12)*		*2.0(12)*		*3.0(12)*	
$N(C_2)$			9.4(13)		1.1(14)		3.8(13)		5.8(13)	
T_{ex}			≤61 K		90 K		81 K		108 K	

LINE	λ (Å)	f-VALUE	HD 147701 W_λ (mÅ)	HD 147701 N (cm^{-2})	20 AQL W_λ (mÅ)	20 AQL N (cm^{-2})	κ AQL W_λ (mÅ)	κ AQL N (cm^{-2})	9 CEP W_λ (mÅ)	9 CEP N (cm^{-2})
$R(0)$	8757.685	1.0(−3)[a]	5.4 ± 1.3[b]	8.0(12)	2.0 ± 0.2	2.9(12)	≤0.5	≤7.4(11)	0.7 ± 0.4	1.0(12)
$N(0)$			8.0(12)		2.9(12)		≤7.4(11)		1.0(12)	
$R(2)$	8753.949	4.0(−4)	7.3 ± 1.4[c]	2.7(13)	5.0 ± 0.4	1.8(13)	≤0.3	≤1.1(12)	0.8 ± 0.4	3.0(12)
$Q(2)$	8761.194	5.0(−4)	3.2 ± 0.8	9.4(12)	7.3 ± 0.5	2.2(13)	≤0.4	≤1.2(12)	0.8 ± 0.3	2.4(12)
$P(2)$	8766.031	1.0(−4)	...	...	≤1.1	≤1.6(13)	...	...	...	...
$N(2)$			9.4(12)		1.8(13)		≤1.1(12)		2.7(12)	
$R(4)$	8751.685	3.33(−4)	3.6 ± 0.5	1.6(13)	3.2 ± 0.2	1.4(13)	≤0.6	≤2.7(12)	≤0.6	≤2.7(12)
$Q(4)$	8763.751	5.0(−4)	7.1 ± 1.0	2.1(13)	5.7 ± 0.5	1.7(13)	2.4 ± 0.3[c]	7.1(12)	...	...
$P(4)$[e]	8773.430	1.67(−4)	2.2 ± 0.8[e]	...	1.8 ± 0.3[e]	...	...	...	...	...
$N(4)$			1.9(13)		1.6(13)		≤2.7(12)		≤2.7(12)	
$R(6)$	8750.848	3.08(−4)	≤1.7	≤8.1(12)	3.0 ± 0.3	1.4(13)	≤0.4	≤1.9(12)	≤1.4	≤6.7(12)
$Q(6)$	8767.759	5.0(−4)	3.0 ± 1.3	8.8(12)	4.2 ± 0.4	1.2(13)	1.8 ± 0.4[c]	5.3(12)	1.4 ± 0.4	4.1(12)
$P(6)$	8782.308	1.92(−4)	≤2.9	≤2.2(13)	3.1 ± 0.6[c]	2.4(13)	...	...	...	...
$N(6)$			8.1(12)		1.3(13)		≤1.9(12)		4.1(12)	
$Q(8)$[e]	8773.221	5.0(−4)	2.7 ± 0.8[e]	7.9(12)	1.1 ± 0.3[e]	3.2(12)	...	...	...	...
$N(8)$			7.9(12)		3.2(12)		...		*1.0(12)*	
$N(10)$			*2.0(12)*		...		...		...	
$N(C_2)$			5.4(13)		5.3(13)		≤6.4(12)		1.2(13)	
T_{ex}			76 K		66 K		...		≤46 K	

[a] $1.0(-3) = 1.0 \times 10^{-3}$.
[b] Subtracted 2.5 mÅ telluric feature seen in other spectra.
[c] Result is suspect because of possible stellar contamination.
[d] Line is contaminated by cosmic-ray hit.
[e] $P(4)$ and $Q(8)$ are blended. $W_\lambda(P4)$ was determined from other $j = 4$ data, from which $W_\lambda(Q8)$ was estimated.
[f] Line is unusually broad.
[g] Column densities in italics are estimated from distribution based on T_{ex}.

the enhancement in the infrared field over the interstellar value. The results for kinetic temperature, which come from T_{ex}, and for density based on the C_2 data are discussed in the sections pertaining to chemical modeling. The density estimates are based on a factor-of-1.8 reduction in $n_c\ \sigma/I_{ir}$ (see note added in proof in van Dishoeck & Black 1982).

For the stars in Cep OB3, the CH and CN column densities were determined by employing a combination of the curve-of-growth method and direct profile integration through the apparent optical depth method (see Savage & Sembach 1991; Savage, Cardelli, & Sofia 1992). Curves of growth were constructed using λλ3886, 4300 for CH. For all the sight lines considered, we typically found $2 < b < 4$ km s^{-1}. The size of these b-values is a consequence of the complex component structure exhibited by the Cep OB3 cloud (see Cardelli, Federman, & Smith 1991). For CN, for which we detected only $R(0)$ (λ3874) absorption and which appeared only at the velocity of the principal CH absorption component, the column densities were derived by assuming $b = 1$ km s^{-1}. The curve-of-growth results were compared with those derived by direct integration of the apparent column density profile, $N_a(v) = 3.768 \times 10^{15} f\lambda\tau_a(v)$, where f is the oscillator strength, λ is the line rest

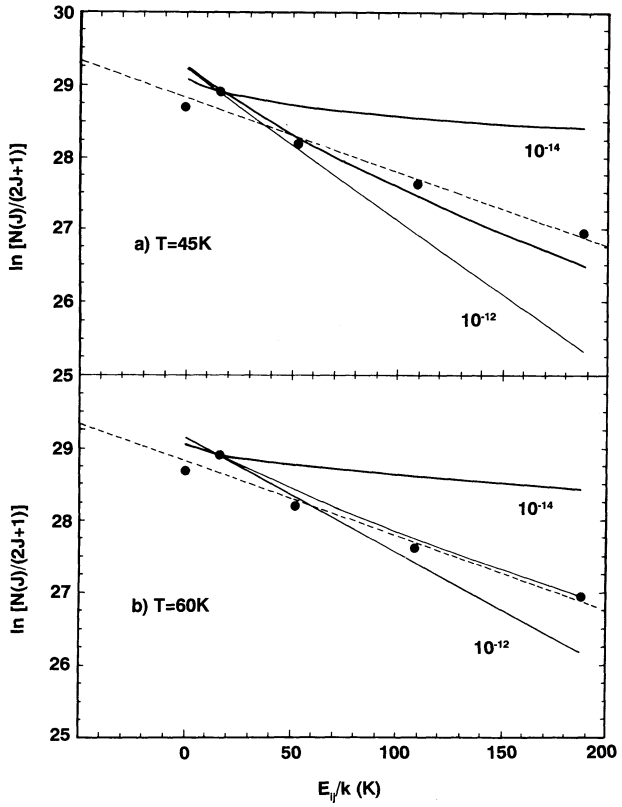

FIG. 2.—Distribution of C_2 rotational levels in the direction of 20 Aql. The dashed lines are a least-squares fit for the excitation temperature, indicating $T_{ex} \sim 66$ K. The solid lines represent theoretical predictions for the distribution based on the work of van Dishoeck & Black (1982); the upper panel shows results for a kinetic temperature of 45 K, while the lower panel shows the case for $T \sim 60$ K. For both kinetic temperatures, the parameter $n_c\ \sigma/I_{ir}$ is approximately 10^{-13}.

wavelength, and $\tau_a(v)$ is the apparent optical depth. In all cases, the results of the $N_a(v)$ integration, including the errors, were consistent with the curve-of-growth results.

4. CHEMICAL ANALYSIS

4.1. *Modeling*

Our chemical analysis is based in large measure on our previous work on CN (Federman et al. 1984; Federman & Lambert 1988) and on C_2 (Federman & Huntress 1989). This analysis incorporates all available information for a sight line, including molecular column densities, observed values for visual and ultraviolet excitation and for the ratio of total-to-selective extinction, and molecular excitation. The major addition was the incorporation of reactions involving NH that lead to CN formation; these were added because the recent discovery of NH in cloud envelopes (Meyer & Roth 1991) indicated significant column densities. The revised rate equations for C_2 and CN in terms of column densities are

$$N(C_2) = \frac{k_1 x(C^+) N(CH) n \alpha}{G(C_2) + k_2 x(O) n + k_3 x(N) n}, \quad (1)$$

and

$$N(CN) = \frac{[k_3 x(N) N(C_2) + k_4 x(N) N(CH) + k_5 x(C^+) N(NH) \alpha] n}{G(CN) + k_6 + x(O) n}. \quad (2)$$

In these equations, the k_i's are reaction rate constants with units $cm^3\ s^{-1}$; $x(X)$ and $N(X)$ are the abundance relative to hydrogen nuclei and the column density of species X; n is the density of hydrogen nuclei, $n(H) + 2n(H_2)$; $G(X)$ is the photodestruction rate of species X; and α is a factor that accounts for the conversion of C^+ into CO (see Federman & Huntress 1989). The rate constants for neutral-neutral reactions include a factor, $(T/300)^{0.5}$, to account for the velocity term in the rate constant. The attenuation of radiation by dust in a cloud is incorporated into the photodestruction rate via the expression, $G(X) = G_0(X) \exp(-\tau_{uv})$, where $G_0(X)$ is the rate at the cloud surface and τ_{uv} is the optical depth of grains at 1000 Å. This wavelength is chosen because it is in the middle of the range (the Lyman limit to 1200 Å) for dissociating C_2 and CN (Pouilly et al. 1983; Lavendy, Robbe, & Gandara 1987). In terms of τ_{uv}, the value for α was obtained from the expression, $\alpha = [1 + 14(\tau_{uv} - 2)/5]^{-1}$, for $\tau_{uv} > 2$ (Federman & Huntress 1989). Table 4 lists the reactions included in our analysis as well as values used for the rates and rate constants. As in previous work, we adopted abundances of 2.5×10^{-4}, 6.9×10^{-5}, and 3.5×10^{-4} for C^+, N, and O, respectively, which indicate modest depletions in cloud envelopes; the factor α accounted for chemical changes in $x(C^+)$. The initial value for τ_{uv} was set at $2\ A_v$, but the final value was determined for a specific cloud by taking into consideration the ratio of total-to-selective extinction, $R = A_v/E(B-V)$, and ultraviolet extinction along the sight line (Cardelli, Clayton, & Mathis 1989) and the clumpiness of material, as seen in maps of dust extinction and molecular emission. The initial value for τ_{uv} is based on the extinction curve of Code et al. (1976) with a reduction of about a factor of 2 to account for preferential forward scattering of the dust. We again rely on rate equations involving column density so that specific portions of the chemistry can be studied in detail for underlying physical and chemical themes. The use of column densities for local densities is an approximation, but likely a reasonable one in light of the fact that molecular abundances increase monotonically with distance into cloud envelopes (see Boland & de Jong 1984). Such a monotonic increase suggests that the chemistry mainly takes place within a restricted volume in a cloud, a view which is reinforced by results described below.

Many reactions involving an ion and a neutral with a large dipole moment have rate constants that increase with decreasing temperature (e.g., Marquette et al. 1985; Rebrion et al. 1988). Both k_1 and k_5 may also show this dependence on tem-

TABLE 4

RATES AND RATE CONSTANTS

Reaction	Rate/Rate Constant	Value ($s^{-1}/cm^3\ s^{-1}$)	Notes
$C^+ + CH \rightarrow C_2^+ + H$	k_1	3.0×10^{-10}	1
		5.1×10^{-10}	2, 3
$C_2 + O \rightarrow CO + C$	k_2	4.0×10^{-11}	4, 5
$C_2 + N \rightarrow CN + C$	k_3	1.7×10^{-11}	2, 5
$CH + N \rightarrow CN + H$	k_4	2.0×10^{-11}	5, 6
$C^+ + NH \rightarrow$ all products	k_5	2.8×10^{-10}	2
		5.6×10^{-10}	2, 3
$CN + O \rightarrow CO + N$	k_6	1.8×10^{-11}	5, 7
$C_2 + h\nu \rightarrow 2C$	$G(C_2)$	2.0×10^{-10}	8
$CN + h\nu \rightarrow C + N$	$G(CN)$	1.0×10^{-10}	9

NOTES.—(1) Federman & Huntress 1989; (2) Derived in this work; (3) Should lower densities apply; (4) Estimate; (5) Rate constant has a temperature dependence of $(T/300)^{0.5}$; (6) Messing et al. 1981; (7) Schmatjko & Wolfrum 1976; (8) Pouilly et al. 1983, corrected for appropriate radiation field; van Dishoeck 1987; (9) Lavendy et al. 1987.

perature. Typical increases between 70 and 25 K are of the order of 20% for molecules with dipole moments similar to those of CH and NH (Rebrion et al. 1988). Furthermore, the predicted trends appear to represent upper bounds for the measured trends (Marquette et al. 1985). Since we were seeking agreement at a level of $\sim$20%, we did not include any temperature dependence for k_1 and k_5.

The chemistry involving NH was incorporated into the calculations in the following manner. The reaction between C^+ and NH has three exothermic, spin-allowed channels: $H^+ + CN$, $CN^+ + H$, and $CH^+ + N$. In previous ion-molecule schemes, usually one channel was considered ($CN^+ + H$ by Prasad & Huntress 1980 and Millar et al. 1991); van Dishoeck & Black (1986) included more than one, but noted that $H^+ + CN$ was the principal route to CN production. Because reactions involving protons as products are limited to very specific cases such as charge exchange (Huntress 1977), we believe that only the channels with molecular ions as products are potential sources of CN from reactions between C^+ and NH. The production of CN^+ is the key ingredient. Although subsequent reactions between CH^+ and N yield CN^+ as a product (Federer et al. 1986), not CN directly as once thought (see Black & Dalgarno 1977), these reactions are too slow (Viggiano et al. 1980; Federer et al. 1986) to compete with the direct production of CN^+ via $C^+ + NH$. Furthermore, ambient CH^+ in the cool, molecular gas has too small an abundance (e.g., van Dishoeck & Black 1986) and reacts with N too slowly to contribute in a significant way to the CN chemistry. Once CN^+ is formed, hydrogen abstraction reactions produce to protonated ions, HCN^+ and H_2CN^+, which recombine with electrons to form CN, among other products. One uncertainty in the scheme remains the branching ratio for CN production. Since most of the HCN produced via $H_2CN^+ + e^-$ will upon dissociation become CN, the overall branching ratio may be close to unity. In any event, the refined value for the rate constant for $C^+ + NH$ that we obtain below can be considered as the product of the actual rate constant and the efficiency of forming CN through products of this reaction. The revised chemical scheme is shown in Figure 3.

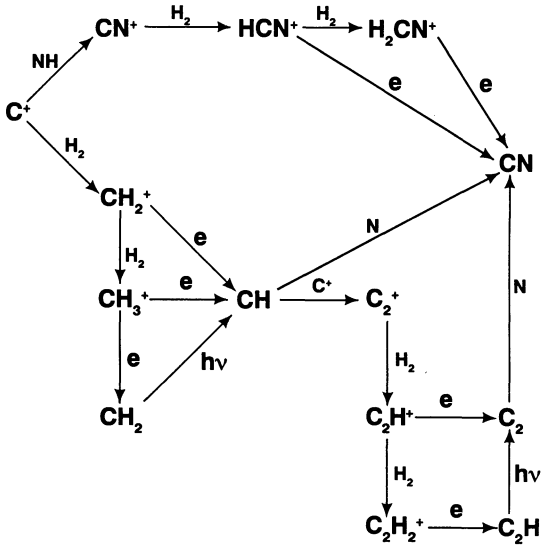

FIG. 3.—The chemical scheme illustrating the most important pathways for the production of CN.

The very weak absorption features of the NH radical have been detected only toward two stars, ζ Per and HD 27778, with respective column densities of 9.0×10^{11} and 2.7×10^{12} cm^{-2} (Meyer & Roth 1991). For these two directions, N(NH) scales approximately as N(CH). Thus, for all other lines of sight in this study we estimated N(NH) from the ratio of N(CH) toward ζ Per and that toward the star in question. This may underestimate N(NH) in the most reddened lines of sight, but for these directions, CN production via reactions involving NH are of secondary importance.

In our previous work, we sought factor of 2 agreement between the observational and theoretical results, but in this study for chemical transitions, we required much closer agreement. In order to obtain the desired agreement, we used the best available information regarding density and temperature (e.g., van Dishoeck & Black 1986; Black & van Dishoeck 1991; van Dishoeck et al. 1991), which usually was derived from detailed studies of rotational excitation in C_2, CO and CN. Our new data for C_2, though less precise than that used in the previous studies, provided a means for verifying our chemical estimates for density and temperature along some sight lines. In the analysis, adjustments from nominal values for density, τ_{uv}, and I_{uv} were made to bring the results into agreement with the data for C_2 and CN. The parameter I_{uv} allows for variations in the local interstellar flux relative to the average interstellar value. Changes in temperature were a less important factor. In most instances, our analyses agreed with observational results at the 20% level, the typical uncertainty associated with the observations.

We focused our attention on three complexes, Sco OB2 and the ρ Oph molecular cloud, Cep OB3 and the cloud Cep A, and stars and dark clouds in the Taurus/Auriga region of the sky. In each of these cases, the sight lines sample dense material (e.g., $200 < n < 1000$ cm^{-3}), not low-density atomic gas; most of the reddening can be ascribed to the envelope of a molecular cloud. Figures 4*a*, 4*b*, and 4*c* show the positions of the program stars and their relation to the molecular gas observed in rotational lines for CO. The outline of the molecular gas is based on the lowest contour in the CO maps, which indicates antenna temperatures of 1–3 K. The maps were obtained by Loren (1989) for the ρ Oph molecular cloud, by Sargent (1979) for the cloud in Cepheus, and by Nercessian et al. (1988b) for the dark clouds in Taurus. In addition to the stellar positions, several dark clouds are also indicated. Of particular note are HCL2 (Heiles cloud 2) which contains TMC-1 (Taurus molecular cloud 1) and L1529 (or TMC-2); HD 29647 samples the envelope of TMC-1 and HD 28975 samples the envelope of TMC-2. At first glance, each environment appears to be different: Cep OB3 contains O stars with H II regions and the molecular cloud appears clumpy; Sco OB2 contains early B stars; and Taurus/Auriga contains mostly late B stars and the gas is very filamentary. Thus an initial goal was to study the effects of environment on chemistry. This turned out to be of secondary importance, however, as revealed by our chemical analyses.

4.2. *Chemical Transitions*

With the modifications to the chemistry described below, chemical transitions were studied. The transitions for C_2 and CN were characterized by depth into the envelope through τ_{uv}, the optical depth from grain attenuation at 1000 Å. For this part of the analysis, typical values for density of 500 cm^{-3} and temperature of 40 K were used.

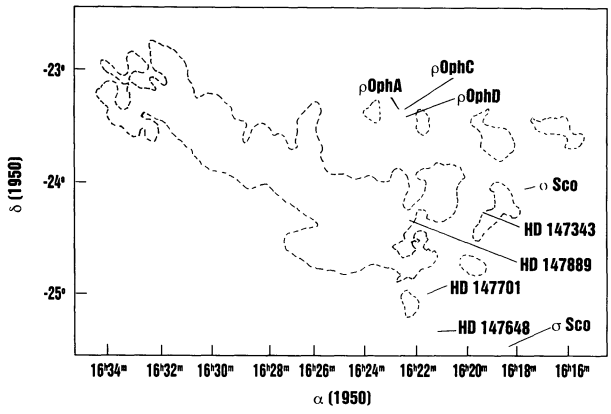

FIG. 4a

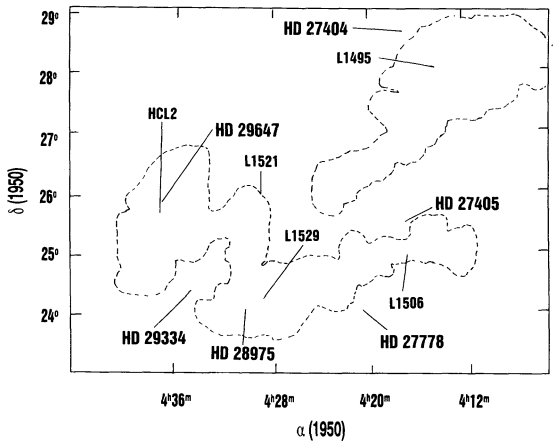

FIG. 4c

FIG. 4.—Maps of molecular emission showing the sight lines that probe the cloud envelope. Only the lowest radio contour is displayed. (*a*) ρ Oph molecular cloud (from ^{13}CO map of Loren [1989] with $T_R^* = 4$ K for the main cloud and 1 K is small isolated regions) and the stars in Sco OB2. (*b*) The molecular cloud in Cepheus (from ^{12}CO study of Sargent [1979] with $T_A^* = 2.5$ K) and stars in Cep OB3. (*c*) Dark clouds in Taurus from ^{13}CO emission with integrated intensities of 1 K km s^{-1} (Nercessian et al. 1988b) and associated stars.

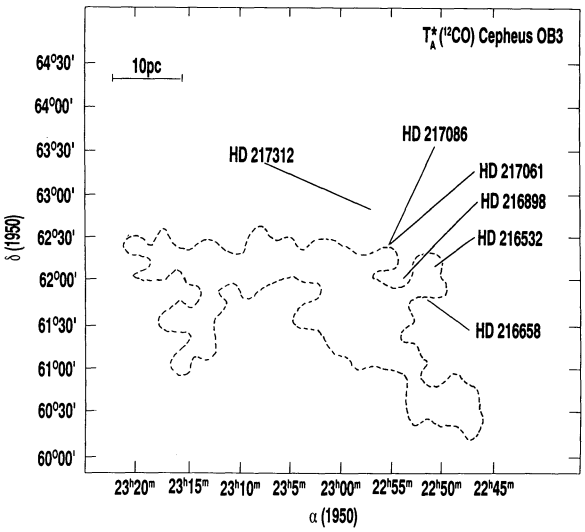

FIG. 4b

Several transitions affect the chemistry of CN; these are indicated in Figure 5, where the column density of CN, N(CN), is plotted against τ_{uv}. The transition at $\tau_{uv} = 2$ arises from the conversion of C^+ into CO. Chemistry for CN involves C^+ because (1) C^+ leads to CH formation; (2) reactions between this ion and CH lead to C_2—both molecules are precursors to CN; and (3) reactions between C^+ and NH result in CN production. The conversion was approximated by the factor α, as suggested by Federman & Huntress (1989). The next transition, which occurs at $\tau_{uv} \sim 3$, also involves production. At lower optical depths, the production of CN is controlled by the ion-molecule reaction $C^+ + NH$, while at larger optical depths the neutral-neutral reactions involving CH and C_2 with N dominate. This transition obviously is also influenced by the depth at which the conversion to CO takes place. At optical depths at 1000 Å of ~4.5, the final transition occurs. Here, destruction via photodissociation is replaced by destruction involving gas-phase collisons. The plateau in the curve at greater optical depths arises because CN is transformed into other molecules through the gas-phase collisions.

Two of these transitions appear in the chemistry for C_2. Since C_2 formation relies on reactions involving C^+, a chemical transition is seen at $\tau_{uv} \sim 2$ as well. The transition among destruction terms also occurs at $\tau_{uv} \sim 4.5$ because the two destruction terms scale in similar ways for these molecules.

These results are quite general, and therefore other situations can be analyzed in terms of them. First, if grain attenuation is less of an effect for a direction of interest, as when the grains show enhanced forward scattering, all chemical transitions would occur deeper into the cloud. How much deeper would depend on the scaling between τ_{uv} and N(H). In a similar vein, changes in I_{uv} can be viewed as rescaled τ_{uv} because $G = I_{uv} G_0 \exp(-\tau_{uv})$. Second, since the range in temperature is not large for the lines of sight studied here—although A_v spans a range of 4 mag—and since portions of the chemistry are independent of T or vary slowly with it, temperature changes are of minor importance for the depth of chemical transitions. Last, variations in density can also be accommodated by the results displayed in Figure 5. For large optical depths, no change occurs in $N(X)$ because both production and destruction involve density (see eqs. [1] and [2]). *Therefore, the plateau at* N(CN) [*and* $N(C_2)$] $\sim 10^{14}$ *cm*$^{-2}$ *is strictly a chemical effect*

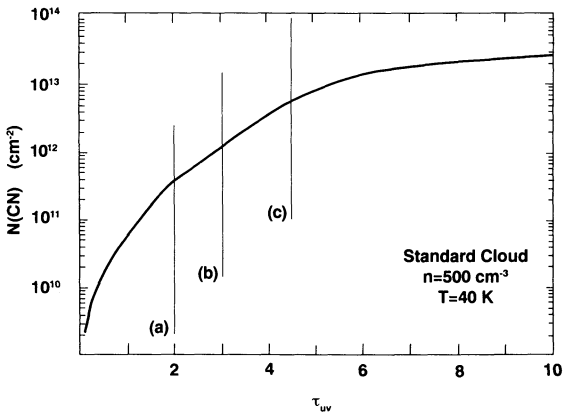

FIG. 5.—A plot of N(CN) vs. τ_{uv} indicating the positions of chemical transitions. (*a*) Where the conversion of C^+ into CO takes place. (*b*) Where production via the ion-molecule reaction $C^+ + NH$ equals production through neutral-neutral reactions involving C_2 and CH with N, with the neutral-neutral reactions dominating at larger τ_{uv}. (*c*) Where photochemical destruction is balanced by gas phase chemical destruction.

independent of physical conditions. When τ_{uv} is small, $N(X)$ scales as n/I_{uv}, and then the discussion regarding variations in I_{uv} applies.

4.3. *Gas toward Sco OB2*

The Sco OB2 association offers us the opportunity to study a variety of environments within a single complex. Both bright, moderately reddened stars, such at ζ Oph, and heavily reddened stars, such as HD 147889, are present. Figure 4*a* shows the relationship between some of the most reddened stars and the ρ Oph molecular cloud. Thus, regions dominated by photochemistry and regions dominated by gas-phase processes can be examined for a single, self-consistent chemical picture. Table 5 shows results for stars in Sco OB2, where density (n), temperature (T), optical depth at 1000 Å (τ_{uv}), enhancement factor for the ultraviolet flux (I_{uv}), observed and predicted column densities, as well as the ratio of observed to predicted column densities, are indicated. The new sources for the observational data are: $N(C_2)$ for HD 147701—the present work; N(CH) and N(CN) for the most reddened stars—Cardelli & Wallerstein (1986); for o Sco—van Dishoeck & Black (1989) and Gredel et al. (1991). For the data studied previously, we adopted the results quoted by Federman et al. (1984), Federman & Lambert (1988), and Federman & Huntress (1989).

The results in Table 5 were achieved through several iterative steps. First, we focused on the most reddened stars because photochemical reactions and ion-molecule reactions involving C^+ would be of little importance. In essence this allowed us to analyze the neutral-neutral chemistry in an isolated manner. Since experimentally determined rate constants exist for the reactions CN + O (Schmatjko & Wolfrum 1976) and CH + N (Messing et al. 1981), the poorly known rate constant for C_2 + N could be determined more precisely. Although it is of little consequence for the most reddened stars, we used a value for τ_{uv} of 1.4 A_v to take into account the presence of large grains, which are inferred from large values for R (Carrasco, Strom, & Strom 1973; Whittet 1974; Vrba et al. 1975). Direct evidence for lower ultraviolet extinction comes from the results of Cardelli et al. (1989), of Fitzpatrick & Massa (1990), and of Snow, Allen, & Polidan (1990), as well as those specifically for HD 147889 (Bohlin & Savage 1981) and for ρ Oph (Green et al. 1992). The exception is the gas toward HD 147648, where in addition to lowering τ_{uv}, we have to increase the UV flux in order to be consistent with the observed upper limit for CN. The observational data are best reproduced when the rate constant k_3 has a value of 1.7×10^{-11} cm^3 s^{-1}, which is one-third the value used in our previous studies (Federman et al. 1984; Federman & Lambert 1988).

We next considered the least reddened stars in Table 5 so that photodestruction and reactions involving C^+ could be treated in a self-consistent manner. For the line of sight toward ζ Oph, the UV extinction is similar to the Galactic average (Bless & Savage 1972; Fitzpatrick & Massa 1990; Snow et al. 1990) and thus τ_{uv} was taken to be 2 A_v. Because both τ_{uv} and I_{uv} affect the amount of photodestruction, an uncertainty that remains in this analysis is which of the two parameters to adjust to bring the predictions into agreement with the observations. For at least reddened stars, we chose to vary I_{uv}, while for the intermediate cases such as o Sco, we allowed both to vary. In order to get the most consistent agreement, the rate constant for the reaction $C^+ + NH$ had to be reduced to 2.8×10^{-10} cm^3 s^{-1}, again a factor of 3 less than previous suggestions (Prasad & Huntress 1980). With these two adjustments, the theoretical results for both the least reddened directions and the intermediate cases are equally good, thereby giving us confidence in the changes and in the general chemical picture. As a result, these refinements in rate constants were applied to our other chemical analyses.

For several of the directions in Sco OB2, other analyses of the physical conditions and chemical makeup are available. First, measurements of C_2 absorption provide estimates for kinetic temperature. The excitation temperature sets an upper limit on the kinetic temperature because the possibility exists for optical pumping of the high-lying rotational levels via infrared radiation (van Dishoeck & Black 1982). A least-squares fit to the distribution of rotational levels observed by us for HD 147701 yields a value for T_{ex} of 76 K. Surely, this is an upper limit to the kinetic temperature, and in our modeling we used T = 50 K. For the most reddened star studied, HD 147889, van Dishoeck and de Zeeuw (1984) obtained T of ~75 K, but it was redetermined to be 55 K (van Dishoeck et al. 1991); our best model was based on T of 40 K. Thus, the excitation temperature of C_2, and hence the kinetic temperatures of the gas, for some of the densest material studied optically are similar in this complex. For o Sco, a star with an intermediate amount of reddening, van Dishoeck et al. quote a value of 40 K for the kinetic temperature, while we used a slightly higher temperature. The results are consistent with each other considering the uncertainties quoted by van Dishoeck et al. Optical absorption from C_2 was also previously detected toward three bright stars, ρ Oph A, χ Oph, and ζ Oph (e.g., Danks & Lambert 1983; van Dishoeck & de Zeeuw 1984). Our kinetic temperatures for the gas toward the bright stars

TABLE 5

MODELING RESULTS FOR GAS TOWARD Sco OB2

Star	n (cm^{-3})	T (K)	τ_{uv}	I_{uv}	N(CH) Observed (cm^{-2})	$N(C_2)$ Observed (cm^{-2})	$N(C_2)$ Predicted (cm^{-2})	Observed / Predicted	N(CN) Observed (cm^{-2})	N(CN) Predicted (cm^{-2})	Observed / Predicted
HD 147889	700	40	4.73	1	1.20(14)[a]	1.20(14)	1.17(14)	1.03	3.50(13)	4.13(13)	0.85
HD 147343	700	40	2.78	1	6.40(13)	...	6.26(13)	...	9.30(12)	9.92(12)	0.94
HD 147648	600	50	3.86	5	6.50(13)	...	1.86(13)	...	<3.90(12)	3.62(12)	1.08
HD 147701	1000	50	3.17	1	5.90(13)	5.40(13)	6.67(13)	0.81	1.50(13)	1.40(13)	1.08
o Sco	600	50	3.21	1	5.00(13)	5.50(13)	4.15(13)	1.32	6.00(12)	9.01(12)	0.67
ρ Oph A	400	50	2.04	1	2.40(13)	2.60(13)	2.25(13)	1.15	2.00(12)	2.34(12)	0.86
ρ Oph C	600	40	2.09	1	2.10(13)	...	2.66(13)	...	2.70(12)	2.86(12)	0.94
χ Oph	400	60	2.30	1	3.40(13)	3.50(13)	2.39(13)	1.47	1.30(12)	3.12(12)	0.42
ζ Oph	400	60	1.98	1	2.50(13)	2.20(13)	2.44(13)	0.90	2.60(12)	2.46(12)	1.06

[a] 1.20(14) = 1.20×10^{14}.

are consistent with the results from C_2; it should be noted that for the gas toward ζ Oph, our results are more consistent with the measurements of Danks & Lambert (1983).

Second, once the kinetic temperature is known, analysis of C_2 excitation then provides an estimate for gas density (van Dishoeck & Black 1982; van Dishoeck et al. 1991). One remaining uncertain factor is the value of the de-excitation cross section for C_2; van Dishoeck & Black suggested a value of 2×10^{-16} cm^2, while Lavendy et al. (1991) and Robbe et al. (1992) recently calculated cross sections about a factor of 2 larger than the previous estimate. Thus use of the more recent results yields correspondingly lower densities. Since most previous determinations of density from C_2 excitation were based on the work by van Dishoeck & Black (1982), we follow this analysis. Their analysis yields $n_c = [n(\mathrm{H}) + n(\mathrm{H_2})]$, but we are more interested in the total density of hydrogen nuclei, $n = [n(\mathrm{H}) + 2n(\mathrm{H_2})]$. For many of the directions with detections of C_2, there appears to be roughly comparable amounts of atomic and molecular hydrogen. Thus we multiply n_c by 1.5 to convert to n. From our data on C_2 for HD 147701, the estimate for density ranges from 400 cm^{-3} to 2100 cm^{-3} for respective kinetic temperatures of 45 and 60 K; this estimate is consistent with the results from our chemical analysis. For other sight lines with estimated densities (see Black & van Dishoeck 1991; van Dishoeck et al. 1991), agreement with our chemical analysis is also satisfactory in large measure because we started with these estimates.

Our results can also be compared with previous detailed chemical analyses (van Dishoeck & Black 1986 for χ and ζ Oph; van Dishoeck & Black 1989 for HD 147889). For the two bright stars, our results for n and T are within the range considered by van Dishoeck & Black (1986). In particular, our densities are in the middle of the ranges found by them. One difference, however, between our results and theirs is that we do not require any enhancement in the ultraviolet field penetrating the cloud; an important consequence is that our predicted amounts of CN agree with the observed ones. Such enhancements were required by them in order to reproduce the populations of high-lying rotational levels of H_2. If another way of populating these levels, such as shock excitation, is operating (e.g., Draine 1986; see also Wagenblast 1992)—the premise we adopt, a less intense ultraviolet field would suffice. In regions dominated by photoprocesses, the molecular abundances scale roughly as n/I_{uv}; thus a factor of 2 increase in the ultraviolet flux can be accommodated within the framework of our chemical results by increasing the density by the same factor. Such a density enhancement would make our results consistent with the high-density results of van Dishoeck & Black (1986). As for gas toward the reddened star HD 147889, van Dishoeck & Black (1989) and we utilized the same data on n and T to formulate a chemical model.

Our chemical analysis reveals a global picture for the gas in the envelope of the ρ Oph molecular cloud for the most part. The densities are somewhat lower, and the temperatures are somewhat higher, in the portion having $A_v \sim 1$ mag. The fact that the more opaque portions have lower temperatures indicates that most of the reddening along the sight line is due to a single cloud complex because the added attenuation from a single cloud reduces heating via photoelectrons. This point is reinforced by kinematic information provided by high-resolution optical observations of the reddened stars (Federman & Lambert, in preparation): In particular, one dominant velocity component is seen in the absorption lines. The denser, more opaque portions probably probe deeper into the molecular cloud. The part of the envelope sampled by C_2 and CN, appears to be in pressure equilibrium with $n_c\, T \sim$ 15,000 to 20,000 cm^{-3} K. The more extended region sampled by CO absorption has a lower density (Sheffer et al. 1992), as expected, but interestingly, the pressure appears to be a factor of 2 or 3 lower than the above estimate. (The region of CO absorption is more extended because of the efficient process of self-shielding.) The difference cannot be attributed to a different ratio for $n(\mathrm{H})/n(\mathrm{H_2})$, because the H I to H_2 transition lies closer to the surface than the C^+ to CO transition. One possible explanation is that turbulent pressure dominates over thermodynamic pressure derived through excitation and chemical considerations. Another intriguing possibility is that the outer portion is *not* in pressure equilibrium with the denser portion of the envelope. This might indicate that the more extended portions are expanding, much like what is found for the atomic halo around the molecular cloud B5 (Andersson, Roger, & Wannier 1992). If the extended portions are expanding, an explanation for the similar kinematic features in CO emission (Crutcher & Federman 1987; Langer, Glassgold, & Wilson 1987; Le Bourlot, Gerin, & Perault 1989) and CN absorption (Lambert, Sheffer, and Crane 1990) is needed.

If the density in the gas sampled by C_2 and CN absorption were halved, the pressure throughout the cloud would be constant. Such a density is obtained when the C_2 excitation cross sections of Lavendy et al. (1991) and Robbe et al. (1992) are utilized. A reanalysis of the chemistry shows that the data for stars in Sco OB2 can be reproduced as well as the data portrayed in Table 5 with slight revisions to the rate constants for $C^+ + CH$ and $C^+ + NH$–$k_1 \rightarrow 5.1 \times 10^{-10}$ cm^3 s^{-1} and $k_5 \rightarrow 5.6 \times 10^{-10}$ cm^3 s^{-1}. Changes in density and rate constants also affect the locations of chemical transitions. The effect of changing n was discussed previously: For a factor of 2 decrease in n, the transition from a photochemical regime to one dominated by gas-phase reactions for both C_2 and CN occurs at $\tau_{\mathrm{uv}} \sim 5$. As for the case of different rate constants, the transition involving production terms in CN chemistry also occurs somewhat deeper into the cloud with $\tau_{\mathrm{uv}} \sim 3.5$. A lower estimate for n based on C_2 excitation would, however, worsen the correspondence among density estimates from excitation of C_2, CN, and CO (see Black & van Dishoeck 1991; Gredel et al. 1991). Without additional constraints on crucial rate constants and T, comparison of the densities from the chemistry and from C_2 excitation cannot presently suggest a preferred cross section. The final resolution to this question of pressure variation requires (1) laboratory measurements of the crucial rate constants and (2) high-quality CO data for other stars to examine whether the results for ζ Oph (Sheffer et al. 1992) are the norm.

4.4. *Gas toward Cep OB3*

The diffuse envelope of the molecular cloud Cep A can be probed by stars in the Cep OB3 association. Figure 4*b* shows the positions of the stars relative to the molecular cloud mapped by Sargent (1979). Polarization measurements reveal normal grain sizes (Coyne, Gehrels, & Serkowski 1974), and this is confirmed in large measure by the fact that the ultraviolet extinction is typical of the general interstellar medium (Massa & Savage 1984; Fitzpatrick & Massa 1990). However, the molecular gas appears clumpy (Sargent 1979), and as a result, the dust distribution is likely to be patchy. We, therefore, chose a value for τ_{uv} of 1.4 A_v to take into account the fact

TABLE 6

MODELING RESULTS FOR GAS TOWARD Cep OB3

Star	n (cm^{-3})	T (K)	τ_{uv}	I_{uv}	N(CH) Observed (cm^{-2})	$N(C_2)$ Observed (cm^{-2})	$N(C_2)$ Predicted (cm^{-2})	Observed / Predicted	N(CN) Observed (cm^{-2})	N(CN) Predicted (cm^{-2})	Observed / Predicted
HD 216532.....	300	65	2.61	1	3.89(13)	...	5.28(12)	...	2.57(12)	2.37(12)	1.08
HD 216658.....	300	65	2.98	1	5.89(13)	...	6.65(12)	...	3.80(12)	4.15(12)	0.92
HD 216898.....	300	65	2.58	1	2.88(13)	...	3.16(12)	...	1.95(12)	1.73(12)	1.13
HD 217061.....	300	65	2.91	1	6.03(13)	...	6.72(12)	...	4.37(12)	4.11(12)	1.06
HD 217086.....	300	65	2.91	3	5.50(13)	...	3.13(12)	...	1.55(12)	1.35(12)	1.15
HD 217312.....	300	65	2.98	3	2.69(13)	...	4.38(12)	...	7.76(11)	6.46(11)	1.20

that the radiation penetrates deeper into a cloud under these circumstances. We considered a relatively low density for the models as well in light of the fact that N(CN) is significantly less for a given N(CH) when compared to many other directions. The results of our modeling effort are shown in Table 6, where the observational data are from this study. Excellent agreement between model predictions and observational results are again evident when n of 300 cm^{-3} and T of 65 K are used. Thus, the pressure of gas probed by CN absorption is constant in the envelope of the molecular cloud Cep A, a result similar to that found for the gas toward Sco OB2. Enhancements in the ultraviolet flux in the directions toward HD 217086 and HD 217312 are needed to account for the extremely small amounts observed for CN because the slight decrease in extinction (Massa & Savage 1984; Fitzpatrick & Massa 1990) is not adequate to explain the large chemical effect. The enhancement cannot be due solely to the flux leaving the stellar surface, because although HD 217086 has the earliest spectral type of the observed stars (O7 V) and is associated with an H II region, HD 217312 has one of the latest spectral types (B0.5 V). Thus the increase in I_{uv} arises from the fact that the star is relatively close to the molecular cloud. In order to improve upon these results, data on other species, especially C_2, are needed.

4.5. *Gas in Taurus/Auriga*

The B stars in Taurus and Auriga probe the envelopes of many of the clouds whose cores have been probed with millimeter-wave observations; Figure 4*c* shows lines of sight from this study that probe the material in the vicinity of Heiles cloud 2. The contours represent the 1 K km s^{-1} limits in ^{13}CO emission (Nercessian et al. 1988b). Of particular note are the lines of sight toward HD 29647 and HD 28975, which pass through the envelopes of the Taurus molecular cloud 1 and the Taurus molecular cloud 2, respectively. Furthermore, HD 27405 and 62 Tau (HD 27778) are behind the outer portions of L1506 (Lynds 1962).

As in the analyses for stars in Sco OB2 and Cep OB3, the chemical analysis started with the physical conditions derived from C_2 and CN excitation. For the sight lines to 62 Tau and AE Aur, we relied on our results for C_2, while for HD 26571, our results on C_2 excitation were combined with those of Black & van Dishoeck (1991) for CN and of van Dishoeck et al. (1991) for CO. The gas density and temperature toward HD 29647 were taken from van Dishoeck et al. (1991) as well.

Our chemical analysis is summarized in Table 7. The model predictions for the most part agree with the observational results to within 30%; the one glaring difference involves CN toward HD 29647, which is discussed in more detail below. In order to obtain the close agreement for the moderately reddened stars, HD 26571 and 62 Tau, the dissociating flux had to be lowered. Through an increase in the amount of ultraviolet extinction over the average value, in which τ_{uv} was set equal to 3 A_v, the predictions for HD 26571 were made consistent with the observations, but the predictions of 62 Tau remained below the observational results. A factor of 2 *reduction* in the incident flux was required to bring modeling results into agreement with the observations. This reduction is likely a consequence of the filamentary nature of the interstellar gas in Taurus, thereby allowing shadowing to take place. Our unpublished measurements of atomic absorption obtained at high spectral resolution reveal several components in many of these sight lines; for instance, we find two equally strong K I components toward 62 Tau, only one of which is associated with molecular material. Of our sample of stars in Taurus and Auriga, extinction curves exist for AE Aur (Fitzpatrick & Massa 1990), which appears to be similar to the average Galactic curve, and for HD 29647 (Cardelli & Savage 1988), which although different from the average curve does not quantitatively affect the chemistry because a large amount

TABLE 7

MODELING RESULTS FOR GAS TOWARD STARS IN TAURUS AND AURIGA

Star	n (cm^{-3})	T (K)	τ_{uv}	I_{uv}	N(CH) Observed (cm^{-2})	$N(C_2)$ Observed (cm^{-2})	$N(C_2)$ Predicted (cm^{-2})	Observed / Predicted	N(CN) Observed (cm^{-2})	N(CN) Predicted (cm^{-2})	Observed / Predicted
HD 24263	400	40	1.44	1.0	9.60(12)	...	5.85(12)	...	5.10(11)	6.03(11)	0.85
HD 26571	1000	20	2.70	1.0	2.00(13)	1.10(14)	8.36(13)	1.32	8.80(12)	1.10(13)	0.80
HD 27405	700	40	2.11	1.0	2.90(13)	...	4.05(13)	...	5.40(12)	4.55(12)	1.19
62 Tau	900	50	3.72	0.5	2.90(13)	3.80(13)	4.23(13)	0.90	1.60(13)	1.71(13)	0.94
HD 28975	200	80	3.17	1.0	2.20(14)	...	5.57(13)	...	1.80(13)	1.23(13)	1.47
HD 29309	500	40	3.10	1.0	5.70(13)[a]	...	4.30(13)	...	5.60(12)	5.75(12)	0.97
HD 29647	700	30	6.76	1.0	1.60(14)	1.50(14)	1.43(14)	1.05	1.60(14)	7.11(13)	2.25
AE Aur	200	60	2.11	1.5	1.20(14)	5.80(13)	3.66(13)	1.58	3.30(12)	4.22(12)	0.78

[a] Since N(CH) is an upper limit, all predicted values are upper limits.

of reddening is present. It should be noted that without knowledge of the extinction curves for the other stars, it is difficult to assign a lower flux to enhanced extinction or to shadowing.

The densities derived from the chemical analysis are within the range suggested by considering molecular excitation. From our results for C_2 toward AE Aur, we obtain $n \sim 300$ cm^{-3}, while the chemical analysis suggests $n \sim 200$ cm^{-3}. The analyses by Black and van Dishoeck (1991) and van Dishoeck et al. (1991) indicate densities in the range 500–2000 cm^{-3} for the gas toward HD 26571, which are consistent with our chemical treatment, $n \sim 1000$ cm^{-3}. The density of approximately 800 cm^{-3} obtained from C_2 excitation is also similar. The temperature of 25 K adopted by Black & van Dishoeck, although consistent with our chemical results, is below the value of ~ 50 K from C_2 excitation. For the envelope toward 62 Tau, the chemical analysis yields $n \sim 900$ cm^{-3}, while our C_2 results indicate a range of 400–800 cm^{-3}. The shadowing of ultraviolet flux suggested by the chemical analysis is not evident at the infrared wavelengths associated with C_2 excitation because extinction is considerably smaller at these longer wavelengths. Finally, our estimate for n of 700 cm^{-3} for the envelope probed by HD 29647 is consistent with the results from molecular excitation, which span a range of 200–2000 cm^{-3} (van Dishoeck et al. 1991).

The envelopes toward HD 147889 and HD 29647 have similar amounts of CH and C_2, but N(CN) is 4 times larger toward HD 29647. This difference is likely the result of two factors. First, dissociation plays a more important role in the gas toward HD 147889; τ_{uv} is lower. Second, a larger fraction of the column toward HD 147889 is low-density gas, as indicated by the large amount of CH^+ in this sight line (Gredel et al. 1993). Cardelli et al. (1990) showed that an inverse correlation exists between $N(CH^+)/N(CH)$ and $N(CN)/N(CH)$. This relationship arises because CH^+ production favors low-density gas, where cooling is limited and destruction is hindered, while CN production favors high-density environments.

In closing this section, we compare the results for the envelopes of TMC-1 and TMC-2, which are seen in absorption against the continua of HD 29647 and HD 28975, respectively. Our chemical results for HD 29647 are very similar to those of Nercessian et al. (1988a) and van Dishoeck & Black (1989). Both stars show similar amounts of CH absorption, but significantly different amounts of CN absorption. Both stars have substantial amounts of reddening, with HD 29647 being somewhat more reddened. From the chemical perspective, the main reason for the differences in N(CN) arises from the differences of a factor of 3 or so lower density ($n \sim 200$ cm^{-3}) in the envelope of TMC-2. The chemical analysis for the gas toward HD 28975 suggests the presence of larger than average grains with a resulting smaller ultraviolet extinction. Larger than average grains are also likely to be present toward HD 29647 (Cardelli & Savage 1988), but photochemistry is not important here. The photometric study by Vrba & Rydgren (1985) revealed a value for R toward HD 29647 that is somewhat larger than average and a typical value toward HD 28975. The values for R are by no means extreme, yet chemical evidence suggests lower than average ultraviolet extinction. Such extinction characteristics are found for dark clouds (Cardelli & Clayton 1991). Moreover, even with the increase in density for TMC-1, our CN predictions, like those of van Dishoeck & Black (1989), fall significantly below the observational results for HD 29647. This may be due to the fact that this line of sight truly probes dark cloud material, and as such, our chemical picture is not complete. Additional evidence for the dark cloud nature of the gas toward HD 29647 comes from the work on ultraviolet extinction (Cardelli & Savage 1988), where the bump is found to be very broad and weak, and from infrared spectroscopy (Whittet et al. 1988), where the 3 μm ice feature is seen toward HD 29647. The stronger radiation field and lower gas density in the direction of HD 28975 probably limits the growth of mantle material, with the result that the 3 μm feature is absent (Whittet et al. 1988).

4.6. *Other Directions*

For completeness, in Table 8 we show results for diffuse gas toward stars in Perseus; many of these stars probe the envelope of the molecular cloud from which the Per OB2 association formed (Sargent 1979). The results for two stars, HD 21483 and ξ Per, are particularly noteworthy; the theoretical results were brought into line with the observations only after adjustments were made to the ultraviolet extinction and incident flux. For HD 21483, more than average extinction, $\tau_{uv} \sim 3\ A_v$, was needed, as was a reduction by a factor of 2 in the incident ultraviolet flux compared to the interstellar value. These adjustments are consistent with other available information. In particular, the extinction curve for this star indicates higher than average far-ultraviolet extinction (Fitzpatrick & Massa 1990), and our unpublished high-resolution K I measurements reveal four components, thereby allowing for the possibility of shadowing taking place in this direction. Analysis of C_2 excitation indicates values for n between 400 and 800 cm^{-3}, while chemical considerations indicate $n \sim 1000$ cm^{-3}. These derived values are consistent with the density derived from CN and CO excitation (Black & van Dishoeck 1991; van Dishoeck et al. 1991). Our gas temperature of 20 K is similar to that adopted by Black & van Dishoeck, but is somewhat less than expected from C_2 excitation. As for ξ Per, the opposite situation best suited the observational data: less extinction ($\tau_{uv} = 1.4\ A_v$) and more flux. Again, observational evidence confirms these modeling predictions. The ultraviolet extinction

TABLE 8

MODELING RESULTS FOR GAS TOWARD STARS IN PERSEUS

Star	n (cm^{-3})	T (K)	τ_{uv}	I_{uv}	N(CH) Observed (cm^{-2})	$N(C_2)$ Observed (cm^{-2})	$N(C_2)$ Predicted (cm^{-2})	Observed / Predicted	N(CN) Observed (cm^{-2})	N(CN) Predicted (cm^{-2})	Observed / Predicted
HD 21291	600	40	2.60	1.0	2.10(13)	...	1.89(13)	...	2.60(12)	2.11(12)	1.23
HD 21483	1000	20	5.21	0.5	4.20(13)	9.40(13)	6.25(13)	1.50	3.70(13)	2.34(13)	1.58
o Per	800	40	1.86	1.0	1.30(13)	2.70(13)	2.19(13)	1.23	2.60(12)	2.65(12)	0.98
ζ Per	700	30	2.05	1.0	2.20(13)	3.50(13)	3.42(13)	1.02	3.90(12)	3.56(12)	1.10
X Per	1000	20	3.84	1.0	3.10(13)	5.30(13)	4.29(13)	1.23	8.40(12)	1.06(13)	0.80
ξ Per	300	70	1.44	1.5	1.10(13)	...	3.35(12)	...	2.60(11)	2.94(11)	0.88

curve for ξ Per is lower than average (Bless & Savage 1972; Snow et al. 1990), and the ultraviolet flux permeating the gas seems to be enhanced (Cardelli et al. 1993). Thus, this discussion provides additional support to the claim that our rate equations must be essentially complete; otherwise, the subtle effects attributed to extinction and flux would not have been apparent. Moreover, van Dishoeck & Black (1986) previously analyzed the chemistry in the gas toward o Per and ζ Per. Our results differ from their results in two ways: (1) we do not require any enhancement in the ultraviolet flux over the average interstellar value; and (2) our gas densities are some 50% higher. Our lower flux and higher density allows us to reproduce the CN observations better. Finally we note that $n_c T$ is restricted to the narrow range of 15,000–20,000 cm^{-3} K for the gas in Perseus sampled by C_2 and CN absorption, a result which is reminiscent of the situation for the envelopes of the ρ Oph molecular cloud and Cep A.

The results for three other interesting lines of sight were analyzed. Cardelli et al. (1990), and subsequently Gredel et al. (1991) and Gredel et al. (1993), found molecular absorption toward HD 62542 from a relatively dense clump of gas associated with the Gum nebula. There is about 1 mag of visual extinction toward the star, but the ultraviolet extinction is much larger than expected for the amount of visual extinction (Cardelli & Savage 1988). Cardelli et al. suggested that the gas density in the clump is at least 1000 cm^{-3} and may be as high as 10^4 cm^{-3}. The sight lines toward 20 Aql and 9 Cep were previously studied by Federman, Strom, and Good (1991), but new observational data allow a more refined examination of the chemistry. In particular, recent data on CN obtained by Hanson, Snow, & Black (1992) toward 20 Aql indicates that N(CN) is lower than the value derived from the results of Frisch (1972), and the present work provides a detection of C_2 absorption toward 9 Cep. It should be noted that new observations by two of us (Federman & Lambert, in preparation) on CN absorption toward 20 Aql are consistent with the results of Hanson et al. (1992).

The observational results for HD 62542 are: $N(\mathrm{CH}) = 3.5 \times 10^{13}$ cm^{-2} (Cardelli et al. 1990); $N(\mathrm{C_2}) = 8 \times 10^{13}$ cm^{-2}; and $N(\mathrm{CN}) = 4.2 \times 10^{13}$ cm^{-2} (Gredel et al. 1991). Cardelli et al. obtained a slightly smaller value for N(CN) of 2.6×10^{13} cm^{-2} because their estimate is based on the somewhat larger excitation temperature. From an analysis of the populations of C_2 rotational levels, Gredel et al. (1993) inferred a density of 500 cm^{-3} and a temperature of 40 K. Even with τ_{uv} set equal to 3 A_v to account for the enhanced ultraviolet extinction seen by Cardelli & Savage (1988), we could not reproduce the large column densities of C_2 and CN with the conditions derived from C_2 excitation. Upon raising the density to 10^4 cm^{-3}, as suggested by Cardelli & Savage, the model results agree somewhat better with the observations—$N(\mathrm{C_2}) = 1.1 \times 10^{14}$ cm^{-2} and $N(\mathrm{CN}) = 3.0 \times 10^{13}$ cm^{-2}. The closest, though not especially good, correspondence arises with the values for k_1 and k_5 based on the models for stars in Sco OB2 with lower densities; then we have $N(\mathrm{C_2}) \rightarrow 1.3 \times 10^{14}$ cm^{-2} and $N(\mathrm{CN}) \rightarrow 2.9 \times 10^{13}$ cm^{-2} for n of 3000 cm^{-3} and T of 30 K. Although the CN results of Gredel et al. (1991) were based on a self-consistent analysis of the B–X and A–X transitions, our chemical models are more consistent with the results by Cardelli et al. (1990), which were based on the B–X transition only. Our analysis suggests two areas for further improvement: (1) measurements of the rate constants k_1 and k_5 and (2) a measurement of NH absorption toward this star. The latter seems particularly worthwhile because reactions involving NH are the principal source of CN and because the visual exctinction is relatively low, but the higher than average ultraviolet extinction indicates more absorption than that toward ζ Per (Meyer & Roth 1991). In any event, it is clear from our analysis that the gas density is indeed high; such a result is not in great conflict with the analysis of Gredel et al. (1993) because the C_2 data are nearly represented by a thermal distribution, from which only a lower limit to the density is possible.

Not only did Hanson et al. (1992) find less CN toward 20 Aql than once thought, they obtained a estimate for density of $\lesssim 10^3$ cm^{-3} from measurements of CO absorption which is inconsistent with the chemical estimate from Federman et al. (1991). Because a smaller value for N(CN) would translate into a lower estimate for density from a chemical perspective, we reanalyzed the available data. In particular, the following observational results were modeled: $N(\mathrm{CH}) = 2.8 \times 10^{13}$ cm^{-2}; $N(\mathrm{C_2}) = 5.3 \times 10^{13}$ cm^{-2}; and $N(\mathrm{CN}) = 4.0 \times 10^{12}$ cm^{-2}. The C_2 results are from this work. Excellent correspondence was achieved when a density of 650 cm^{-3}, a temperature of 50 K, and an average value for τ_{uv} of 2 A_v were used; the ratios of observed-to-predicted column densities were 1.20 and 0.74 for C_2 and CN, respectively. The conclusion here is that estimates of density from chemical considerations and from C_2 and CO excitation are now in agreement.

Finally, with the detection of C_2 toward 9 Cep [$N(\mathrm{C_2}) = 1.2 \times 10^{13}$ cm^{-2}], the chemistry toward this star can be analyzed more carefully. With observed column densities of 2.8×10^{13} cm^{-2} and 1.7×10^{12} cm^{-2}, respectively, for CH and CN, our modeling results are $N(\mathrm{C_2}) = 1.4 \times 10^{13}$ cm^{-2} and $N(\mathrm{CN}) = 2.2 \times 10^{12}$ cm^{-2} for n of 300 cm^{-3} and T of 35 K. The ultraviolet extinction appears to be similar to the Galactic average, as indicated by results for the nearby star λ Cep (Snow et al. 1990), and so τ_{uv} equals 2 A_v. Because NH plays a very important role in the production of CN along this sight line, our new results are based on a somewhat lower density than that inferred by Federman et al. (1991). Another way of reproducing the observations is to keep n at 500 cm^{-3}, while raising I_{uv} a factor of 2. Since Federman et al. found no enhancement in the dust temperature toward the star, which would be another manifestation of a larger ultraviolet flux, the model incorporating a lower density is the preferred one.

5. DISCUSSION

Our results regarding the chemistry of C_2 and CN in cloud envelopes reveal that the basic reaction schemes are essentially complete. Although we considered a restricted chemistry containing only the most important reactions, our model predictions reproduce the observations remarkably well. The densities derived from this effort agree with those obtained from C_2 and CN excitation, as well as those from other, more detailed chemical analyses. One difference between our results for the lines of sight to the least reddened stars and previous studies (e.g., van Dishoeck & Black 1986) is that we do not require any significant enhancement in the ultraviolet flux over the interstellar value. A small enhancement can be accommodated by a corresponding increase in density. One consequence of this difference is that we are able to reproduce the observed column density of CN, and a second consequence is that the rate constant for the radiative association reaction, $\mathrm{C^+ + H_2 \rightarrow CH_2^+ + } h\nu$, may be lower than once thought. Our value of 1×10^{-16} cm^3 s^{-1} is more compatible with the value

used in modeling dark clouds (Boland & de Jong 1984). Moreover, the relatively large value for I_{uv} used in the analysis of Sheffer et al. (1992) for fractionation and excitation of CO toward ζ Oph may arise from underestimates in the photodissociation rate for CO (see van Dishoeck & Black 1988), and not necessarily from an enhanced field. For example, recent results for the E–X transition (Stark et al. 1992) suggest somewhat larger cross sections than those used in the past, and many transitions have only lower limits for predissociation widths (F. Rostas, private communication). Although previous calculations of CO self-shielding took most predissociation probabilities to be unity, a lower limit for predissociation widths also yields an upper limit for the optical depth at line center, thereby allowing radiation to penetrate deeper into a cloud.

Sims et al. (1992) recently reported that the neutral-neutral reaction, CN + O_2, has a rate constant varying inversely with temperature as $T^{-0.6}$. They suggested that if the neutral-neutral reactions in our chemical scheme (see Fig. 3) have no appreciable barrier to complex formation, the rate constants will vary in a similar manner with temperature, not as $T^{0.5}$, which is based solely on considerations of velocity. The premise could be tested by looking at the effects on C_2 chemistry for sight lines with large n and/or τ_{uv}. Since both production and destruction of CN at large n and/or τ_{uv} involve neutral-neutral reactions, a study of the temperature dependence is not possible. For kinetic temperatures spanning 30 to 40 K, the size of the increase in C_2 destruction from the use of the inverse temperature dependence ranges from a factor of 12 to one of 6. At the present time, the combined uncertainties in the parameters of equation (1)—k_1 $N(CH)\alpha/k_2x(O)$—appear to be too large to make a definitive statement.

We are able to obtain agreement between observational results and theoretical predictions at the 20% level in most instances. This level of agreement is somewhat surprising in light of the remaining uncertainties, such as in the abundance of C^+ and in chemical rates, in our simple model. However, the fact that our modeling efforts reproduced data for cloud envelopes with varying amounts of extinction and that predictions of the strength of the ultraviolet radiation field in several examples were confirmed by other pieces of observational data gives us confidence in the validity of our model. The possibility exists, therefore, that the remaining uncertainties offset each other.

The analyses of the chemistry as a whole and the chemical transitions involving the production and destruction of C_2 and CN provide further insight into the observed global trends among CH, C_2, and CN. In particular, we comment on the relationships N(CN) versus $N(C_2)$, N(CN) versus N(CH), and $N(C_2)$ versus N(CH) (see Fig. 6 through 8). The data for these plots are tabulated in the Appendix. For our linear regression analysis with censored data, we relied on the package ASURV-Rev. 1.1 (see Isobe, Feigelson & Nelson 1986; Isobe & Feigelson 1990; La Valley, Isobe, & Feigelson 1992). When limits existed for the dependent variable only, the Buckley-Jones method was employed, and when limits existed for both variables, the Schmitt method was used. We have confidence in the derived fits because the results did not differ significantly from those of an analysis where each data point was treated as a detection.

A surprising result from our plots is that the strongest correlation exists between log N(CN) and log $N(C_2)$—see Figure 6. A slope of 1.56 $\pm$ 0.09 is found from a weighted average of four

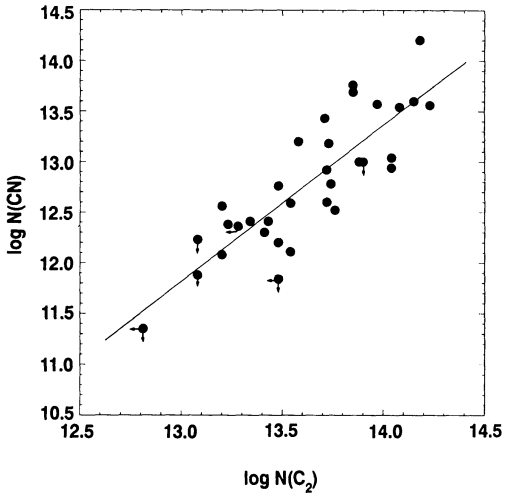

FIG. 6.—A logarithmic plot of N(CN) vs. $N(C_2)$. The solid line is a fit that includes a treatment of limits—see text for description.

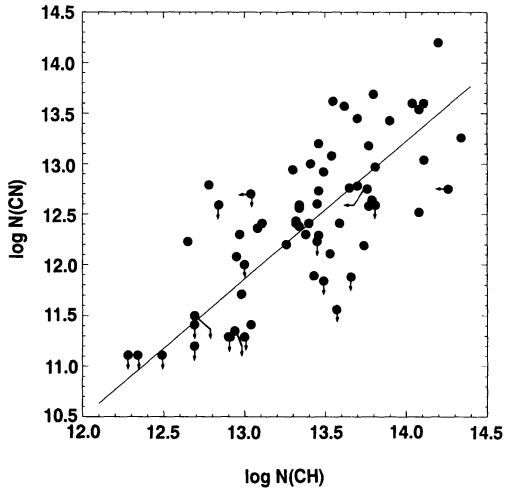

FIG. 7.—Same as Fig. 6 for N(CN) vs. N(CH)

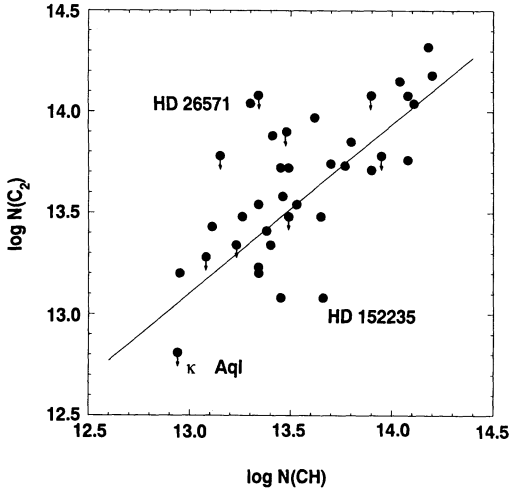

FIG. 8.—Same as Fig. 6 for $N(C_2)$ vs. N(CH). The sight lines with extreme values for $N(X)$ are indicated.

computations of the Schmitt method with different binning. Of the 33 data points, six of them were limits, but the individual analyses revealed that two to four of these limiting values were consistent with detections. If all the data were detections, a least-squares fit yields a slope of 1.55 ± 0.18 and a correlation coefficient of 0.85. The other two plots show weaker correspondences. For the plot log N(CN) versus log N(CH) (Fig. 7), the Schmitt method yields a slope from the weighted average of three similar computations of 1.37 ± 0.09. Here a least-squares fit, which treats all data as detections, gives a somewhat smaller slope of 1.16 ± 0.13 and correlation coefficient of 0.74. Van Dishoeck & Black (1989) noted the general trend seen in a plot of log $N(C_2)$ against log N(CH). With our larger database, we find a roughly linear relationship with a slope of 0.83 ± 0.15 based on the Buckley-Jones method for the data in Figure 8. If all the data were detections, the slope would be 0.70 ± 0.13, and the correlation coefficient would be 0.67. Since the results from techniques accommodating limits and those from a simple least-squares fit are most similar for the plot of N(CN) versus $N(C_2)$, this is indeed the strongest among the three relationships.

In hindsight these results can be understood from a perspective where correlations between species arise from chemical considerations *and* from instances when species coexist within a volume of gas (see Federman, Huntress, & Prasad 1990). The strong correlation between CN and C_2 in Figure 6 naturally comes from the fact that C_2 and CN occupy similar volumes (or clumps) within a cloud. Chemistry does not play a significant role in the strength of this correlation because CN production proceeds through three paths whose individual contributions depend on τ_{uv} (see Fig. 5). The reason for the strong correlation—spatial coexistence—is consistent with our finding described above that the pressure of the gas sampled by C_2 and CN is similar for various lines of sight in a cloud or complex. The dispersion about the least-squares fit in Figure 6 is predominantly the result of observational error.

The weaker correspondences found in the other two cases arise in large measure because CH absorption samples a much more extended portion of the cloud with a lower average density when compared to the situation for the other two molecules. In particular, the tight correlation between N(CH) and $N(H_2)$ (Federman 1982; Danks et al. 1984; Mattila 1986) is a consequence of the extended volume over which CH is observed. The amount of CH associated with the region sampled by C_2 and CN absorption, which probably varies from one sight line to another, cannot be discerned with confidence at this time. A potential method for extracting the appropriate amount of CH involves are more definitive, laboratory-based value for the rate constant k_1: From the observed column density for C_2, equation (1) can be inverted and solved for N(CH). A somewhat lower value for N(CH) would not affect the results from equation (2) in any significant way because only about 30% of the production of CN comes from reactions between CH and N.

The slope of ~ 1.5 in Figure 6, however, originates from the chemistry. If the correlation between the two molecules were solely an effect of spatial coexistence, a linear relationship would be expected, but that is not found. Instead, in envelopes with large amounts of C_2, the increase in N(CN) occurs faster than the increase in $N(C_2)$. From a chemical perspective, in regions where the amount of C_2 increases, the importance of CN production via C_2 increases. In particular, for lines of sight dominated by photochemistry, such as that toward ζ Oph, C_2 plays a minor role ($\sim 15\%$) in CN production, but when photochemical reactions are not important, such as toward HD 147889, the contribution from C_2 is about 35%. This variation, when added to the linear correspondence from occupying similar volumes, leads to a slope greater than unity. Similarly, the slope of ~ 1.3 in the relationship between log N(CN) and log N(CH) (Fig. 7) is related to chemistry. As in the case for C_2 reactions, the contribution from CH reactions to CN chemistry increases with increasing N(CH). For the two lines of sight discussed above, the contribution increases from 15 to 40%. The probable reason for a slope that is intermediate between the slopes for the other two relationships involves the combined effects of CH reactions producing CN directly and indirectly through C_2.

The column density ratio $N(C_2)/N$(CH), or equivalently the slope of ~ 1.0 in Figure 8, also has a chemical basis: C_2 formation via CH reactions with C^+. When most of the C_2 destruction involves photodissociation, equation (1) becomes

$$N(C_2) = \frac{k_1 x(C^+) n}{G(C_2)} N(CH) \sim N(CH) . \quad (3)$$

On the other hand, when gas-phase reactions dominate,

$$N(C_2) \rightarrow \frac{k_1 x(C^+) \alpha}{k_2 x(O)} N(CH) , \quad (4)$$

which is this limit also goes to N(CH). The dispersion in this plot is predominantly due to variations in $x(C^+)$, n, and $G(C_2)$ when n and/or τ_{uv} are small and to variations in $x(C^+)$ through the parameter α when n and/or τ_{uv} are large. There appears to be more dispersion in Figure 8 when N(CH) is small; this may be due to the fact that some of the dispersion for small N(CH) arises from CH extending beyond the region (clump) seen in C_2. Lines of sight with substantial amounts of CH, on the other hand, seem to have smaller fractions of the extended CH.

In light of the correlations involving these carbon compounds, two other observational facts deserve mention. First, Wannier et al. (1993) recently showed that in strip maps across dark clouds, OH emission and its abundance relative to total hydrogen nuclei peak in the vicinity of the atomic-to-molecular hydrogen transition in cloud envelopes, not in the cloud interior where CO emission originates. Since CH and OH are the first neutral molecules formed in their respective chemical networks, their distribution is expected to be widespread. Second, Federman (1981) noted that column densities of neutral atoms, such as Na I and C I, show stronger correlations with $N(H_2)$ than with column densities of H I or total hydrogen nuclei. This too is a spatial correspondence because large abundances of neutral atoms are present only in regions where the ultraviolet flux has been attenuated and/or where the density is somewhat higher; such regions also occur in the vicinity of the H I/H_2 transition within a cloud envelope.

For completeness, a plot of log N(CO) versus log N(CH) based on all available data (see Appendix) is shown in Figure 9. For $N(CH) \leq 3 \times 10^{13}$ cm^{-2}, the quadratic dependence noted previously (e.g., Federman & Lambert 1988) is still evident. The new piece of information is that for several directions with large N(CH), a jump in N(CO) from 10^{15} cm^{-2} to $\sim 10^{18}$ cm^{-2} takes place. This marks the threshold where CO self-shielding becomes important and where C^+ is effectively converted into CO. Using the relationship between N(CH) and A_v described by Federman (1982) and Mattila (1986), $N(CH) \sim 2 \times 10^{13}$ cm^{-2} A_v, most of the carbon is transformed

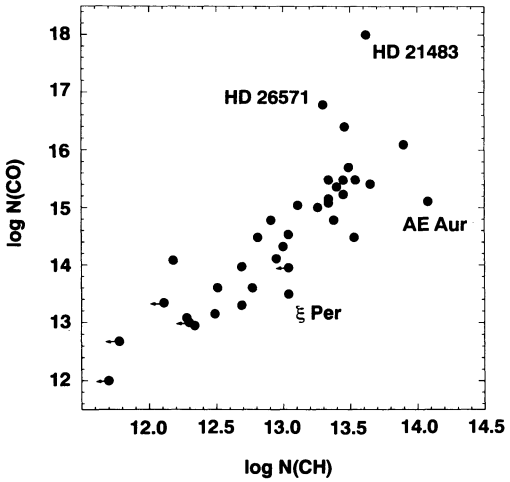

FIG. 9.—A plot of log N(CO) vs. log N(CH). The sharp increase in N(CO) for N(CH) $\sim 3 \times 10^{13}$ cm^{-2} may indicate where CO self-shielding suppresses molecular destruction. Again, extreme examples are indicated.

into CO at $A_v \sim 3$ mag or $\tau_{uv} \sim 6$, a result which is consistent with the compilation by Federman et al. (1990) of radio data. The direction toward AE Aur, however, does not appear to follow the trend for other sight lines with significant amounts of CH; the reason for the difference may lie in the fact that high-resolution observations toward AE Aur reveal several components with substantial amounts of neutral material (Federman & Lambert, in preparation). As a result, the molecular material is distributed over several interstellar cloud envelopes. Another possibility centers on the relatively low density derived from the chemical analysis above (to explain the small amount of CN); under such circumstances, self-shielding is less effective because fewer CO molecules are produced.

Thus the following picture emerges regarding the volume sampled by various species. Because of self-shielding, H_2 samples most of the cloud envelope. Since CH is the first neutral hydrocarbon formed in the chemical network (see Fig. 3), and since self-shielding is also important for CO chemistry, the region observed via CH and CO absorption is somewhat less extensive. Finally, C_2 and CN are restricted to the inner regions of cloud envelopes, because these molecules form after additional chemical reactions involving CH have taken place and, therefore, are susceptible to photodissociation of progenitor molecules as well as their own photodissociation.

A final point involves the apparent decrease is observed CN abundance in denser and more opaque regions than those probed here (see Crutcher, Churchwell, & Ziurys 1984; Nyman & Millar 1989). Such an effect is expected because this diatomic molecule will be transformed into more complex species in a denser, more shielded environment. The same picture applies, for example, to the OH results of Wannier et al. (1993): The OH abundance is high only in regions where the molecule has not been converted into CO, O_2, and other species.

6. CONCLUSIONS

The findings of this study are briefly summarized here. An analysis of the chemistry for C_2 and CN in cloud envelopes reveals three transitions: one involving the conversion of C^+ into CO at $\tau_{uv} \sim 2$; a second one at $\tau_{uv} \sim 3$ pertaining to the production mechanisms for CN, and one at $\tau_{uv} \sim 4.5$ where photodissociation is balanced by gas-phase reactions. Analytical expressions were used to model the observations of C_2 and CN toward stars in Sco OB2, Cep OB3, and Taurus/Auriga; in most instances the agreement between model predictions and observational results is at the 20% level. This close correspondence between theory and experiment and the similar estimates of density and temperature from both molecular excitation and chemical analysis suggest that the chemistry of these carbon species in cloud envelopes is reasonably well understood. Moreover, the pressures derived from these estimates of density and temperature seem to be constant within a cloud envelope regardless of opacity in the region. Finally, the observational data show a stronger correlation when log N(CN) is plotted against log $N(C_2)$ than when the results for N(CN) and $N(C_2)$ are plotted against log N(CH). This arises because CN and C_2 occupy a similar volume. The distribution of CH, on the other hand, is more widespread.

Several avenues are being pursued to clarify the issues raised in our analysis. Observations of CO absorption toward other stars will provide information on whether density or pressure estimates from CO are systematically lower than those from C_2 and CN measurements. Strip maps of CH 9 cm emission across the envelopes of dark clouds will show the extent of the CH distribution. Laboratory measurements on rate constants for ion-molecule reactions involving radicals such as CH and NH and measurements of NH absorption from a larger sample of directions are planned. These measurements are crucial because they will eliminate two of the weakest links in the analysis. Finally, high-resolution, high signal-to-noise data on C_2 and CN will aid in understanding the excitation for these molecules.

We thank Greg Crinklaw, who obtained and reduced several spectra, and Yaron Sheffer, who assisted in deriving column densities, and we acknowledge the help of Vince Anicich and Eric Herbst, who provided information on chemical reactions. We also thank Bob Loren, Anneila Sargent, and Yves Viala for allowing us to use their CO maps. S. R. F. was supported, in part, by the NASA RTOPs program and funded through the Jet Propulsion Laboratory and by the Faculty Research Awards and Fellowships Program of the University of Toledo. D. L. L. was supported by grant no. NSF 91-15090 from the National Science Foundation, J. A. C. acknowledges support from NASA-LTSARP grant NAGW-2520.

APPENDIX

A compilation of data on CH, CO, C_2, CN, and H_2 through approximately 1992 January is shown in Table 9. For the most part, only ground-based observations obtained with solid-state detectors are included, while the ultraviolet data predominantly come from measurements with the *Copernicus* satellite and *IUE*. For H_2, the data come from Savage et al. (1977) and Bohlin, Savage, & Drake (1978); otherwise, the source is indicated in the table. Our previous compilations (e.g., Federman et al. 1984) list earlier references. The column densities for the carbon-bearing molecules were derived from the measured equivalent widths by considering

TABLE 9

COMPILATION OF MOLECULAR RESULTS

HD	STAR	log N(X) CH	Reference	CO	Reference	C_2	Reference	CN	Reference	H_2
2905	κ Cas	12.90	1	...	...	...	...	$\leq$11.29	2	20.27
21278	...	...	...	13.58	3	...	...	...	...	19.48
21291	...	13.32	4	...	...	...	...	12.41	4	...
21483	...	13.62	4	18.00	5	13.97	4	13.57	4, 6	...
23180	o Per	13.11	1	15.04	7	13.43	8	12.41	2	20.61
23408	20 Tau	12.18	1	14.08	3	...	...	...	...	19.75
23512	...	12.84	4	...	...	...	...	$\leq$12.59	4	...
23552	...	...	...	15.59	9	...	...	...	...	...
24263	...	12.98	10	...	...	...	...	11.71	10	...
24398	ζ Per	13.34	1	15.08	11	13.54	8	12.59	2	20.67
24534	X Per	13.49	12	15.70	13	13.72	12	12.92	12	21.04
24760	ϵ Per	$\leq$12.30	1	13.00	3	...	...	...	...	19.52
24912	ξ Per	13.04	1	13.49	14	...	...	11.41	2	20.53
25154	...	13.61	10	...	...	...	...	...	...	...
26571	...	13.30	4, 15	16.78	5	14.04	4	12.94	15	...
27405	...	13.46	4	...	...	...	...	12.73	4	...
27778	62 Tau	13.46	4	16.40	5	13.58	4	13.20	4, 16	...
28975	...	14.34	4	...	...	...	...	13.26	4	...
29309	...	$\leq$13.76	4	...	...	...	...	12.75	4	...
29334	...	13.72	4	...	...	...	...	...	...	...
29647	...	14.20	17	...	...	14.18	18, 19	14.20	17	...
30614	α Cam	12.81	1	14.48	20	...	...	...	...	20.34
34078	AE Aur	14.08	4	15.11	21	13.76	4	12.52	4	...
36665	...	...	...	15.11	22	...	...	...	...	...
36861	λ Ori	...	...	13.80	20	...	...	...	...	19.11
37318	...	...	...	14.15	23	...	...	...	...	...
37903	...	$\leq$13.04	4	13.95	5	...	...	$\leq$12.70	4	...
41117	χ^2 Ori	13.04	24	14.53	25	...	...	...	...	...
47129	...	12.95	26	14.11	25	...	...	...	...	20.54
48099	...	12.57	26	...	...	...	...	...	...	20.29
53367	...	$\leq$14.26	4	...	...	...	...	12.75	4, 28	...
54662	...	13.05	26	...	...	...	...	...	...	20.00
62542	...	13.55	27	...	...	...	...	13.62	27, 28	...
63804	...	...	...	...	...	14.23	29	13.56	28, 29	...
72088	...	12.89	30	...	...	...	...	...	...	...
72350	...	13.04	30	...	...	...	...	...	...	...
72648	...	13.41	30	...	...	...	...	...	...	...
73658	...	12.83	30	...	...	...	...	...	...	...
73882	...	14.11	4	...	...	...	...	13.60	4, 28	...
75149	...	13.23	26	...	...	$\leq$13.34	29	...	...	...
78344	...	...	...	...	...	13.90	29	$\leq$13.00	29	...
80077	...	14.04	29	...	...	14.15	29	13.60	28, 29	...
92740	...	12.68	26	...	...	...	...	...	...	19.97
93160	...	12.93	30	...	...	...	...	...	...	...
93161	W	13.15	30	...	...	...	...	...	...	...
93161	E	13.28	30	...	...	...	...	...	...	...
94413	...	...	...	...	...	13.85	29	13.76	28, 29	...
110432	...	13.26	29, 31	15.00	32	13.48	29	12.20	28, 29	...
112244	...	12.69	26	...	...	...	...	$\leq$11.50	2	20.14
113904	θ Mus	12.04	26	...	...	...	...	...	...	19.83
115842	...	13.34	26	...	...	$\leq$14.08	29	...	...	...
143018	π Sco	$\leq$11.70	26	12.00	3	...	...	...	...	19.32
143275	δ Sco	12.34	26	12.95	33	...	...	$\leq$11.11	2	19.41
144217	β^1 Sco	12.28	1, 26	13.08	33	...	...	$\leq$11.11	2	19.83
144470	ω^1 Sco	12.51	1, 26	13.60	33	...	...	...	...	20.05
145502	ν Sco	12.77	1, 26	13.60	33	...	...	...	...	19.89
147009	...	13.08	4	...	...	...	...	...	...	...
147084	o Sco	13.70	29	...	...	13.74	29	12.78	28, 29	...
147165	σ Sco	12.49	1, 26	13.15	33	...	...	$\leq$11.11	2	19.79
147343	...	13.81	34	...	...	...	...	12.97	34	...
147648	...	13.81	34	...	...	...	...	$\leq$12.59	34	...
147701	...	13.77	34	...	...	13.73	4	13.18	34	...
147888	ρ Oph D	13.46	4	...	...	...	...	...	...	...
147889	...	14.08	29, 34	...	...	14.08	35	13.54	34	...
147932	ρ Oph C	13.32	4	...	...	...	...	12.43	4	...
147933	ρ Oph A	13.38	26	14.78	33	13.41	8	12.30	2	20.57
148184	χ Oph	13.53	26	14.48	36	13.54	8, 35	12.11	2	20.63
149038	μ Nor	13.00	26	14.32	3	...	...	$\leq$11.29	2	20.44
149404	...	...	...	15.54	25	...	...	12.28	28	...
149757	ζ Oph	13.40	26	15.36	37	13.34	8	12.41	2	20.65

TABLE 9—*Continued*

HD	Star	log N(X) CH	Reference	CO	Reference	C_2	Reference	CN	Reference	H_2
151804	...	12.70	26	...	...	...	...	...	...	20.26
152234	...	12.95	38	...	...	13.20	39	12.08	39	...
152235	...	13.66	38	...	...	13.08	39	≤11.88	39	...
152236	...	13.34	38	15.48	25	13.20	29	12.56	39	...
152248	...	13.00	38	...	...	...	...	≤12.00	39	...
152249	...	12.65	38	...	...	...	...	12.23	39	...
152270	...	13.08	38	...	...	≤13.28	39	12.36	39	...
152408	...	12.72	26	...	...	...	...	...	...	20.38
152424	...	13.57	38	...	...	...	...	≤11.56	39	...
154368	...	13.90	29	16.09	40	13.71	35	13.43	28, 29, 41	...
156738	...	13.48	29	...	...	≤13.90	29	...	...	...
157038	...	13.49	42	...	...	≤13.48	29	≤11.84	42	...
157246	γ Ara	≤11.78	26	12.68	43	...	...	...	...	19.24
161056	B	...	...	...	...	...	...	12.81	28	...
161056	A	...	...	...	...	...	...	12.48	28	...
164353	67 Oph	12.69	1, 26	13.30	3	...	...	≤11.20	2	20.26
166734	...	13.95	29	...	...	≤13.78	29	...	...	...
167263	16 Sgr	12.72	26	...	...	...	...	...	...	20.18
167264	15 Sgr	12.69	26	13.97	25	...	...	≤11.41	2	20.28
168183	...	...	...	15.23	44	...	...	...	...	...
168607	...	13.15	29	...	...	≤13.78	29	...	...	...
	BD −14°5037	14.11	4, 29	...	...	14.04	45	13.04	28, 29	...
169454	...	13.80	4, 29	...	...	13.85	29, 45	13.69	4, 28, 29	...
169754	...	13.90	29	...	...	≤14.08	29	...	...	...
170740	...	12.78	46	...	...	...	...	12.79	28	...
	TY CrA	13.70	47	...	...	...	...	13.45	47	...
179406	20 Aql	13.45	48	15.48	48	13.72	4	12.60	48	...
184915	κ Aql	12.94	1	...	...	≤12.81	4	≤11.35	2	20.31
190603	...	13.04	49	...	...	...	...	...	...	...
193322	...	[a]	...	14.34	25	...	...	≤12.00	50	20.08
229059	...	14.36	29	...	...	...	...	...	...	...
	Cyg OB2 No. 12	...	...	...	...	14.64	19	...	...	...
199579	...	12.97	24	...	...	...	...	12.30	50	20.36
200120	59 Cyg	...	...	12.85	3	...	...	...	...	19.30
200775	...	13.64	4	...	...	...	...	...	...	...
203064	68 Cyg	12.91	1	14.78	25	...	...	≤11.29	2	20.29
206165	9 Cep	13.45	2	13.23	25	13.08	4	≤12.23	2	...
206267	...	13.41	2	...	...	13.88	12	13.00	2	...
207198	...	13.65	2	15.41	5, 12	13.48	12	12.76	2	...
210072	...	...	...	...	...	...	...	12.97	4	...
210121	...	13.54	51, 52	15.48	52	...	...	13.08	28, 52	...
210839	λ Cep	13.34	2	15.15	25	13.23	12	12.38	2	20.78
216532	...	13.59	4	...	...	...	...	12.41	4	...
216658	...	13.77	4	...	...	...	...	12.58	4	...
216898	...	13.46	4	...	...	...	...	12.29	4	...
217061	...	13.79	4	...	...	...	...	12.64	4	...
217086	...	13.74	4	...	...	...	...	12.19	4	...
217312	...	13.43	4	...	...	...	...	11.89	4	...
217675	o And	≤12.11	1	13.34	3	...	...	...	...	19.67
218376	1 Cas	12.88	1	...	...	...	...	...	...	20.15
218662	...	13.32	53	...	...	...	...	...	...	...
224572	σ Cas	12.54	1	...	...	...	...	...	...	20.23
	BD +66°1675	14.18	29	...	...	14.32	19	...	...	...

[a] CH is a trace (see Frisch 1972).

References.—(1) Federman 1982; (2) Federman et al. 1984; (3) Federman et al. 1980; (4) This work; (5) Joseph et al. 1986; (6) Meyer et al. 1990; (7) Snow 1975; (8) Danks & Lambert 1983; (9) Tarafdar 1983; (10) Penprase et al. 1990; (11) Snow 1977; (12) Federman & Lambert 1988; (13) Lien et al. 1981; (14) Smith et al. 1991; (15) Crawford 1990a; (16) Meyer & Roth 1991; (17) Crutcher 1985; (18) Hobbs et al. 1983; (19) Lutz & Crutcher 1983; (20) Jenkins et al. 1973; (21) McLachlan & Nandy 1984; (22) Gondhalekar & Phillips 1980; (23) Phillips & Gondhalekar 1983; (24) Frisch 1972; (25) Tarafdar & Krishna Swamy 1982; (26) Danks et al. 1984; (27) Cardelli et al. 1990; (28) Gredel et al. 1991; (29) van Dishoeck & Black 1989; (30) Wallerstein & Gilroy 1992; (31) Crawford 1991; (32) Codina et al. 1984; (33) Snow & Jenkins 1980; (34) Cardelli & Wallerstein 1986; (35) van Dishoeck & de Zeeuw 1984; (36) Frisch 1980; (37) Sheffer et al. 1992; (38) Crawford 1989; (39) Crawford 1990b; (40) Dickman et al. 1983; (41) Palazzi et al. 1990; (42) Hawkins & Meyer 1989; (43) Morton & Hu 1975; (44) Welsh 1984; (45) Gredel & Münch 1986; (46) Gredel et al. 1993; (47) Cardelli & Wallerstein 1989; (48) Hanson et al. 1992; (49) Allen & Snow 1992; (50) Joseph et al. 1989; (51) de Vries & van Dishoeck 1988; (52) Welty & Fowler 1992; (53) Welty et al. 1989.

$b = 1$ km s^{-1}, as mentioned above. For CO, the additional assumption that T_{ex} is 4 K was made. Since new laboratory measurements of band oscillator strengths for the C–X and E–X transitions of CO (Krishnakumar & Srivastava 1986; Eidelsberg et al. 1991; Stark et al. 1992; F. Rostas, private communication) are available, we reexamined the appropriate f-values for use in the compilation. This body of work indicates that $f_{00}(C–X)$ is 0.075 and $f_{00}(E–X)$ is 0.042; these f-values are somewhat smaller than those used by Federman et al. (1980). With the revised values, results from the survey of Federman et al. for directions with detections of relatively weak lines in both transitions are found to be self-consistent. Another point regarding CO observations is worth mentioning here. Although radio observations may sample a larger volume than absorption-line measurements because the radio telescope beam has a finite size, our column densities from CO absorption in the A–X band toward HD 26571 and HD 154368 are consistent with the multitransition radio study of van Dishoeck et al. (1991). For HD 21483, however, our suggested value for N(CO) is about a factor of 10 larger than that quoted by them; this difference could be due either to inappropriate values for T_{ex} and b in our derivation or to smoothing of the emission over the larger radio beam.

Since 1992, January several other papers on optical absorption have appeared, including those by Gredel et al. (1992, 1993) and Jenniskens, Ehrenfreund, & Désert (1992). Of particular note are the CH results of Jenniskens et al. for stars in common with our survey and of Gredel et al. (1993) for HD 73882 and HD 53367, where we estimated N(CH) from λ3878. With regard to the work of Jenniskens et al., the W_λ's for the A–X transition toward HD 21483 are in excellent agreement, and their result for λ4300 toward AE Aur is consistent with our results for $\lambda\lambda$3886, 3890. As for the comparison with Gredel et al. for HD 73882, our W_λ for λ3878, though somewhat larger than theirs, is consistent when measurement errors are taken into account. Their column density from λ4300 is significantly smaller than our estimate from λ3878, but considering that we have a marginal detection, we cannot discern whether or not our suggestion of multiplying the column density of the $T_{2e}(\frac{1}{2})$ state by 3 is appropriate for the few directions with only a measurement of λ3878. For the other direction in common with Gredel et al., we have only an upper limit. In any event, we plan on maintaining and updating Table 9 as new data become available; those interested in obtaining the most recent version of the Table should contact S. R. F.

REFERENCES

Allen, M. M., & Snow, T. P. 1992, ApJ, 391, 152
Andersson, B.-G., Roger, R. S., & Wannier, P. G. 1992, A&A, 260, 355
Bally, J., & Langer, W. D. 1982, ApJ, 255, 143
Black, J. H., & Dalgarno, A. 1977, ApJS, 34, 405
Black, J. H., & van Dishoeck, E. F. 1991, ApJ, 369, L9
Bless, R. C., & Savage, B. D. 1972, ApJ, 171, 293
Bohlin, R. C., & Savage, B. D. 1981, ApJ, 249, 109
Bohlin, R. C., Savage, B. D., & Drake, J. F. 1978, ApJ, 224, 132
Boland, W., & de Jong, T. 1984, A&A, 134, 87
Cardelli, J. A., & Clayton, G. C. 1991, AJ, 101, 1021
Cardelli, J. A., Clayton, G. C., & Mathis, J. S. 1989, ApJ, 345, 245
Cardelli, J. A., Federman, S. R., & Smith, V. V. 1991, ApJ, 381, L17
Cardelli, J. A., Mathis, J. S., Ebbets, D. C., & Savage, B. D., 1993, ApJ, 402, L17
Cardelli, J. A., & Savage, B. D. 1988, ApJ, 325, 864
Cardelli, J. A., Suntzeff, N. B., Edgar, R. J., & Savage, B. D. 1990, ApJ, 362, 551
Cardelli, J. A., & Wallerstein, G. 1986, ApJ, 302, 492
———. 1989, AJ, 97, 1099
Carrasco, L., Strom, S. E., & Strom, K. M. 1973, ApJ, 182, 95
Code, A. D., Davis, J., Bless, R. C., & Hanbury Brown, R. 1976, ApJ, 203, 417
Codina, S. J., de Freitas Pacheco, J. A., Lopes, D. F., & Gilra, D. 1984, A&AS, 57, 239
Coyne, G. V., Gehrels, S. J. T., & Serkowski, K. 1974, AJ, 79, 581
Crawford, I. A. 1989, MNRAS, 241, 575
———. 1990a, MNRAS, 243, 593
———. 1990b, MNRAS, 244, 646
———. 1991, A&A, 246, 210
Crutcher, R. M. 1985, ApJ, 288, 604
Crutcher, R. M., Churchwell, E., & Ziurys, L. M. 1984, ApJ, 283, 668
Crutcher, R. M., & Federman, S. R. 1987, ApJ, 316, L71
Danks, A. C., Federman, S. R., & Lambert, D. L. 1984, A&A, 130, 62
Danks, A. C., & Lambert, D. L. 1983, A&A, 124, 188
de Vries, C. P., & van Dishoeck, E. F. 1988, A&A, 203, L23
Dickman, R. L., Somerville, W. B., Whittet, D. C. B., McNally, D., & Blades, J. C. 1983, ApJS, 53, 55
Draine, B. T. 1986, ApJ, 310, 408
Eidelsberg, M., Benayoun, J. J., Viala, Y., & Rostas, F. 1991, A&AS, 90, 231
Federer, W., Villinger, H., Lindinger, W., & Ferguson, E. E. 1986, Chem. Phys. Lett., 123, 12
Federman, S. R. 1981, A&A, 96, 198
———. 1982, ApJ, 257, 125
Federman, S. R., Danks, A. C., & Lambert, D. L. 1984, ApJ, 287, 219
Federman, S. R., & Glassgold, A. E. 1980, A&A, 89, 113
Federman, S. R., Glassgold, A. E., Jenkins, E. B., & Shaya, E. J. 1980, ApJ, 242, 545
Federman, S. R., Glassgold, A. E., & Kwan, J. 1979, ApJ, 227, 466
Federman, S. R., & Huntress, W. T. 1989, ApJ, 338, 140
Federman, S. R., Huntress, W. T., & Prasad, S. S. 1990, ApJ, 354, 504
Federman, S. R., & Lambert, D. L. 1988, ApJ, 328, 777
Federman, S. R., Strom, C. J., & Good, J. C. 1991, AJ, 102, 1393
Fitzpatrick, E. L., & Massa, D. 1990, ApJS, 72, 163
Frisch, P. C. 1972, ApJ, 173, 301
———. 1980, ApJ, 241, 697
Glassgold, A. E., Huggins, P. J., & Langer, W. D. 1985, ApJ, 290, 615
Glassgold, A. E., & Langer, W. D. 1975, ApJ, 197, 347
Gondhalekar, P. M., & Phillips, A. P. 1980, MNRAS, 191, 13P
Gredel, R., & Münch, G. 1986, A&A, 154, 336
Gredel, R., van Dishoeck, E. F., & Black, J. H. 1991, A&A, 251, 625
———. 1993, A&A, 269, 477
Gredel, R., van Dishoeck, E. F., de Vries, C. P., & Black, J. H. 1992, A&A, 257, 245
Green, J. C., Snow, T. P., Cook, T. A., Cash, W. C., & Poplawski, D. 1992, ApJ, 395, 289
Hanson, M. M., Snow, T. P., & Black, J. H. 1992, ApJ, 392, 571
Hawkins, I., & Meyer, D. M. 1989, ApJ, 338, 888
Hobbs, L. M., Black, J. H., & van Dishoeck, E. F. 1983, ApJ, 271, L95
Huntress, W. T. 1977, ApJS, 33, 495
Isobe, T., & Feigelson, E. D. 1990, BAAS, 22, 917
Isobe, T., Feigelson, E. D., & Nelson, P. I. 1986, ApJ, 306, 490
Januzzi, B. T., Black, J. H., Lada, C. J., & van Dishoeck, E. F. 1988, ApJ, 332, 995
Jenkins, E. B., Drake, J. F., Morton, D. C., Rogerson, J. B., Spitzer, L., & York, D. G. 1973, ApJ, 181, L122
Jenniskens, P., Ehrenfreund, P., & Désert, F.-X. 1992, A&A, 265, L1
Joseph, C. L., Snow, T. P., & Seab, C. G. 1989, ApJ, 340, 314; erratum, 347, 561
Joseph, C. L., Snow, T. P., Seab, C. G., & Crutcher, R. M. 1986, ApJ, 309, 771
Krishnakumar, E., & Srivastava, S. K. 1986, ApJ, 307, 795
Lambert, D. L., Sheffer, Y., & Crane, P. 1990, ApJ, 359, L19
Langer, W. D., Glassgold, A. E., & Wilson, R. W. 1987, ApJ, 322, 450
La Valley, M., Isobe, T., & Feigelson, E. D. 1992, BAAS, 24, 839
Lavendy, H., Robbe, J. M., Chambaud, G., Levy, B., & Roueff, E. 1991, A&A, 251, 365
Lavendy, H., Robbe, J. M., & Gandara, G. 1987, J. Phys. B, 20, 3067
Le Bourlot, J., Gerin, M., & Perault, M. 1989, A&A, 219, 179
Lien, D., Buhl, D., Crutcher, R. M., Donn, B., Smith, A. M., Snyder, L. E., & Stief, L. J. 1981, The Universe at Ultraviolet Wavelengths, ed. R. D. Chapman (NASA CP-2171), 581
Loren, R. B. 1989, ApJ, 338, 902
Lutz, B. L., & Crutcher, R. M. 1983, ApJ, 271, L101
Lynds, B. T. 1962, ApJS, 7, 1
Marquette, J. B., Rowe, B. R., Dupeyrat, G., Poissant, G., & Rebrion, C. 1985, Chem. Phys. Lett., 122, 431
Massa, D., & Savage, B. D. 1984, ApJ, 279, 310
Mattila, K. 1986, A&A, 160, 157
McLachlan, A., & Nandy, K. 1984, MNRAS, 207, 355
Messing, I., Filseth, S. V., Sadowski, C. M., & Carrington, T. 1981, J. Chem. Phys., 74, 3874
Meyer, D. M., & Roth, K. C. 1991, ApJ, 376, L49
Meyer, D. M., Roth, K. C., & Hawkins, I. 1990, ApJ, 343, L1
Millar, T. J., Rawlings, J. M. C., Bennett, A., Brown, P. D., & Charnley, S. B. 1991, A&AS, 87, 585
Morton, D. C., & Hu, E. 1975, ApJ, 202, 638
Münch, G. 1968, in Nebulae & Interstellar Matter, ed. B. M. Middlehurst & L. H. Aller (Chicago: Univ. Chicago Press), 365
Nercessian, E., Benayoun, J. J., & Viala, Y. P. 1988a, A&A, 195, 245
Nercessian, E., Castets, A., Cernicharo, J., & Benayoun, J. J. 1988b, A&A, 189, 207

Nyman, L.-Å, & Millar, T. J. 1989, A&A, 222, 231
Palazzi, E., Mandolesi, N., Crane, P., Kutner, M. L., Blades, J. C., & Hegyi, D. J. 1990, ApJ, 357, 14
Penprase, B. E., Blades, J. C., Danks, A. C., & Crane, P. 1990, ApJ, 365, 241
Phillips, A. P., & Gondhalekar, P. M. 1983, MNRAS, 202, 483
Pouilly, B., Robbe, J. M., Schamps, J., & Roueff, E. 1983, J. Phys. B, 16, 437
Prasad, S. S., & Huntress, W. T. 1980, ApJ, 239, 151
Rebrion, C., Marquette, J. B., Rowe, B. R., & Clary, D. C. 1988, Chem. Phys. Lett., 143, 130
Robbe, J. M., Lavendy, H., Lemoine, D., & Pouilly, B. 1992, A&A, 256, 679
Sargent, A. I. 1979, ApJ, 233, 163
Savage, B. D., Bohlin, R. C., Drake, J. F., & Budich, W. D. 1977, ApJ, 216, 291
Savage, B. D., Cardelli, J. A., & Sofia, U. J. 1992, ApJ, 401, 706
Savage, B. D., & Sembach, K. R. 1991, ApJ, 379, 245
Schmatjko, K. J., & Wolfrum, J. 1976, 16th Symposium (International) on Combustion, (Pittsburgh: The Combustion Institute), 819
Sheffer, Y., Federman, S. R., Lambert, D. L., & Cardelli, J. A. 1992, ApJ, 397, 482
Sims, I. R., Queffelec, J. L., Defrance, A., Rebrion-Rowe, C., Travers, D., Rowe, B. R., & Smith, I. W. M. 1992, J. Chem. Phys., 97, 8798
Smith, A. M., Bruhweiler, F. C., Lambert, D. L., Savage, B. D., Cardelli, J. A., Ebbets, D. C., Lyu, C.-H., & Sheffer, Y. 1991, ApJ, 377, L61
Snow, T. P. 1975, ApJ, 201, L21
———. 1977, ApJ, 216, 724
Snow, T. P., Allen, M. M., & Polidan, R. S. 1990, ApJ, 359, L23
Snow, T. P., & Jenkins, E. B. 1980, ApJ, 241, 161
Stark, G., Smith, P. L., Ito, K., & Yoshino, K. 1992, ApJ, 395, 705
Strömgren, B. 1948, ApJ, 108, 242
Tarafdar, S. P. 1983, MNRAS, 204, 1081
Tarafdar, S. P., & Krishna Swamy, K. S. 1982, MNRAS, 200, 431
van Dishoeck, E. F. 1987, in IAU Symposium 120, Astrochemistry, ed. M. S. Vardya & S. P. Tarafdar (Dordrecht: Reidel), 51
van Dishoeck, E. F., & Black, J. H. 1982, ApJ, 258, 522
———. 1986, ApJS, 62, 109
———. 1988, ApJ, 334, 771
———. 1989, ApJ, 340, 273
van Dishoeck, E. F., Black, J. H., Phillips, T. G., & Gredel, R. 1991, ApJ, 366, 141
van Dishoeck, E. F., & de Zeeuw, T. 1984, MNRAS, 206, 383
Viala, Y. P., Letzelter, C., Eidelsberg, M., & Rostas, F. 1988a, A&A, 193, 265
Viala, Y. P., Roueff, E., & Abgrall, H. 1988b, A&A, 190, 215
Viggiano, A. A., Howarka, F., Albritton, D. L., Fehsenfeld, F. C., Adams, N. G., & Smith, D. 1980, ApJ, 236, 492
Vrba, F. J., & Rydgren, A. E. 1985, AJ, 90, 1490
Vrba, F. J., Strom, K. M., Strom, S. E., & Grasdalen, G. L. 1975, ApJ, 197, 77
Wagenblast, R. 1992, MNRAS, 259, 155
Wallerstein, G., & Gilroy, K. K. 1992, AJ, 103, 1346
Wannier, P. G., Andersson, B.-G., Federman, S. R., Lewis, B. M., Viala, Y. P., & Shaya, E. 1993, ApJ, 407, 163
Welsh, B. Y. 1984, MNRAS, 207, 167
Welty, D. E., & Fowler, J. R. 1992, ApJ, 393, 193
Welty, D. E., Hobbs, L. M., Blitz, L., & Penprase, B. E. 1989, ApJ, 346, 232
White, R. E. 1984, ApJ, 284, 685
Whittet, D. C. B. 1974, MNRAS, 168, 371
Whittet, D. C. B., Bode, M. E., Longmore, A. J., Adamson, A. J., McFadzean, A. D., Aitken, D. K., & Roche, P. F. 1988, MNRAS, 233, 321